

Pittsburg State University

## Pittsburg State University Digital Commons

---

Electronic Theses & Dissertations

---

Spring 12-11-2021

### Polymeric Nanofibers Supported Metal Oxides for Electrochemical Energy Storage Devices

Rutul Patel

Pittsburg State University, rutulpatel2394@gmail.com

Follow this and additional works at: <https://digitalcommons.pittstate.edu/etd>

 Part of the [Polymer Science Commons](#)

---

#### Recommended Citation

Patel, Rutul, "Polymeric Nanofibers Supported Metal Oxides for Electrochemical Energy Storage Devices" (2021). *Electronic Theses & Dissertations*. 409.  
<https://digitalcommons.pittstate.edu/etd/409>

This Thesis is brought to you for free and open access by Pittsburg State University Digital Commons. It has been accepted for inclusion in Electronic Theses & Dissertations by an authorized administrator of Pittsburg State University Digital Commons. For more information, please contact [digitalcommons@pittstate.edu](mailto:digitalcommons@pittstate.edu).

POLYMERIC NANOFIBERS SUPPORTED METAL OXIDES FOR  
ELECTROCHEMICAL ENERGY STORAGE DEVICES

A Thesis Submitted to the Graduate School  
In Partial Fulfillment of the Requirements  
For The Degree of Master of Science

Rutul Patel

Pittsburg State University

Pittsburg, Kansas

December 2021

POLYMERIC NANOFIBERS SUPPORTED METAL OXIDES FOR  
ELECTROCHEMICAL ENERGY STORAGE DEVICES

Rutul Patel

APPROVED:

Thesis Advisor

\_\_\_\_\_  
Dr. Ram Gupta, Department of Chemistry

Committee Member

\_\_\_\_\_  
Dr. Khamis Siam, Department of Chemistry

Committee Member

\_\_\_\_\_  
Dr. Jody Neef, Department of Chemistry

Committee Member

\_\_\_\_\_  
Dr. John Franklin, English and Modern Languages Department

## ACKNOWLEDGMENTS

First and foremost, I give my special thanks to Dr. Ram Gupta for the invaluable assistance he has shown throughout my research. He has been greatly significant, especially expressing his compassion to his students. Again, I acknowledge him for inspiring many students through his mentorship talks, and thus he has enabled the students to become autonomous and self-confident. I have benefited from his mentorship conversation that has made me develop self-efficacy. He has encouraged me to overcome difficult situations in my life. I positively compliment his commitment towards creating a serene and enabling environment to improve my learning skills. Without his contribution, I would not have reached this far.

My family has also been helpful all through. Basically, I would thank my parents and sisters for the much support they have shown me. They have given me abundant support, especially for helping me secure the chance to study abroad. Again, I would thank my family when I was undertaking my research project.

I would also appreciate the support I have received from Dr. Franklin, Dr. Khamis Siam, and Dr. Neef for my thesis committee. I am grateful to the entire Department of Chemistry for their financial support when I was undertaking the project, and basically helping me complete this phase of my journey at Pittsburg State University without any significant inconveniences. Lastly, I would share my gratitude to the people I have met in this town and the warm reception they have shown me.

# POLYMERIC NANOFIBERS SUPPORTED METAL OXIDES FOR ELECTROCHEMICAL ENERGY STORAGE DEVICES

An Abstract of the Thesis by  
Rutul Patel

With increasing demand for energy, there is an increased need to find effective ways to store the available energy to sustain current and future generations. Thus, the research investigates whether polymeric nanofibers support metal oxide are a good solution to store energy. The materials used for synthesis includes N-dimethylformamide, nickel nitrate, cobalt nitrate and polyacrylonitrile.

These fibers are developed three phases. First, a homogenous mixture is prepared, followed by electrospinning of the mixture. Next, calcination of the prepared nanofibers was done to generate the 1D nanofibers embedded with metal oxides. The samples are primarily tested for supercapacitor applications, hydrogen evolution reactions and oxygen evolution reactions.

The findings of the experiment were that, for the oxygen evolution reaction (OER), NiO exhibited an overpotential of 380 mV. After sulfurization, the overpotential changed from 380 mV to 311 mV. For the hydrogen evolution reaction (HER), a combination of NiO and  $\text{Co}_3\text{O}_4$  has shown the overpotential of 96 mV, which was almost unchanged after sulfurization. The fabricated materials were effective for HER and OER applications. Typically, about 300 mV overpotential for the OER materials are considered appropriate materials for commercial application. The material fabricated in the experiment (sulfurized nickel oxide) exhibit an overpotential of 311 mV for OER application, for which is counted and thus deemed an outstanding outcome. The best material for HER application is

platinum, which demonstrates the overpotential of 70 mV. Again, one of the materials fabricated (combination of NiO and Co<sub>3</sub>O<sub>4</sub>) for the experiment showed overpotential of 96 mV. Any material that exhibits an overpotential under 100 mV is considered an effective material for the HER application. For supercapacitor applications, sulfurized NiO showed specific capacitance of 215 F/g.

Sulfurized nickel oxide showed good results for OER and Super capacitor applications, however mixture of nickel oxide and cobalt oxide shows good results for the HER application.

## TABLE OF CONTENTS

<b>CHAPTER I</b> .....	1
1.1 Introduction .....	1
1.2 Renewable Energy Sources .....	3
1.2.1 Wind Energy .....	3
1.2.2 Hydropower Energy .....	3
1.2.3 Geothermal Energy .....	4
1.2.4 Solar Energy .....	4
1.3 Energy Storage Devices .....	5
1.3.1 Battery .....	5
1.3.2 Fuel Cell .....	6
1.3.3 Capacitors .....	7
1.3.3.1 Electric Double Layer Capacitors .....	7
1.3.3.2 Pseudo Capacitors .....	8
1.3.3.3 Hybrid Capacitors .....	9
1.4 Materials Used for Energy Application .....	9
1.4.1 Types of Nanomaterials .....	9
1.4.1.1 Carbon Derived Nanomaterials .....	10
1.4.1.2 Inorganic Nanomaterials .....	10
1.4.1.3 Organic Nanomaterials .....	10
1.4.1.4 Composite-based Nanomaterials .....	10
1.4.2 Division on the Basis of Dimensions .....	11
1.4.3 Division Based on the Origin .....	12
1.4.3.1 Natural Nanomaterials .....	12
1.4.3.2 Synthetic Nanomaterials .....	13
1.4.4 Use of Nanomaterials .....	13
1.5 Properties of Capacitors .....	14
1.5.1 Specific Capacitance .....	14
1.5.2 Energy and Power Density .....	15
1.5.3 Ragone Plot .....	15
1.6 Electrolysis .....	16
1.6.1 Water Splitting Technology .....	17
1.7 Objective of the Thesis .....	18
<b>CHAPTER II</b> .....	20
2.1 Experimental Details .....	20
2.1.1 Materials Used .....	20
2.1.2 Preparation of 1D Nanofibers: .....	20
2.1.2.1 First Stage .....	20
2.1.2.2 Second Stage .....	21
2.1.2.3 Third Stage .....	23
2.1.3 Sulfurization .....	23
2.1.4 Ni Foam Preparation .....	24
2.1.5 Electrode Making .....	24

2.1.6 Electrochemical Measurements .....	25
2.1.6.1 Cyclic Voltammetry .....	26
2.1.6.2 Electrochemical Impedance Spectroscopy .....	27
2.1.6.3 Linear Sweep Voltammetry .....	27
2.1.6.4 Chronoamperometry .....	28
2.1.7 Tafel Slope.....	28
2.1.8 Electrochemical Stability Test.....	29
<b>CHAPTER III</b> .....	30
3.1 Result and Discussion .....	30
3.1.1 Cyclic Voltammetry .....	30
3.1.2 Galvanostatic Charge-Discharge Analysis .....	37
3.1.3 Electrocatalyst for Oxygen Evolution Reaction .....	44
3.1.4 Electrocatalyst for Hydrogen Evolution Reaction.....	48
3.1.5 Tafel Slope.....	53
3.1.6 Electrochemical Impedance Spectroscopy .....	54
3.1.7 Scanning Electron Microscope .....	58
3.1.8 Electro Chemical Stability Test.....	67
3.1.9 Electrochemical Stability Test for Supercapacitor .....	71
<b>CHAPTER IV</b> .....	77
4.1 Conclusions .....	77
<b>REFERENCES</b> .....	79

## LIST OF TABLES

Table 2.1: Experimental details for the synthesis of nanofibers.....	24
Table 3.1: Calculate specific capacitance from CV curve.....	37

## LIST OF FIGURES

Figure 1.1: Fuel cell .....	6
Figure 1.2: Schematic representation of electric double layer capacitors .....	8
Figure 1.3: Ragone plot for various energy devices .....	16
Figure 2.1: Four different compositions used to prepare homogeneous solutions for different samples .....	21
Figure 2.2: Electrospinning process.....	22
Figure 2.3: Electrospinning and calcination .....	23
Figure 2.4: Cyclic voltammogram .....	26
Figure 2.5: Three electrode test .....	27
Figure 2.6: Linear sweep voltammetry .....	28
Figure 3.1: CV curves of PAN sample at various scan rates .....	33
Figure 3.2: CV curves of S-PAN sample at various scan rates .....	33
Figure 3.3: CV curves of NiO sample at various scan rates .....	34
Figure 3.4: CV curves of S-NiO sample at various scan rates.....	34
Figure 3.5: CV curves of Co <sub>3</sub> O <sub>4</sub> sample at various scan rates.....	35
Figure 3.6: CV curves of S-Co <sub>3</sub> O <sub>4</sub> sample at various scan rates .....	35
Figure 3.7: CV curves of NiO-Co <sub>3</sub> O <sub>4</sub> sample at various scan rates.....	36
Figure 3.8: CV curves of S-NiO-Co <sub>3</sub> O <sub>4</sub> sample at various scan rates .....	36
Figure 3.9: Scan rate versus specific capacitance.....	37
Figure 3.10: Potential versus time at different current density for PAN .....	39
Figure 3.11: Potential versus time at different current density for S-PAN.....	40
Figure 3.12: Potential versus time at different current density for NiO .....	40
Figure 3.13: Potential versus time at different current density for S-NiO.....	41
Figure 3.14: Potential versus time at different current density for Co <sub>3</sub> O <sub>4</sub> .....	41
Figure 3.15: Potential versus time at different current density for S-Co <sub>3</sub> O <sub>4</sub> .....	42
Figure 3.16: Potential versus time at different current density for NiO-Co <sub>3</sub> O <sub>4</sub> .....	42
Figure 3.17: Potential versus time at different current density for S-NiO-Co <sub>3</sub> O <sub>4</sub> .....	43
Figure 3.18: Specific capacitance versus current density for unsulferized sample .....	43
Figure 3.19: Specific capacitance versus current density for sulferized sample .....	44
Figure 3.20: LSV curves of PAN at 1 and 1000 cycles.....	45
Figure 3.21: LSV curves of S-PAN at 1 and 1000 cycles. ....	46
Figure 3.22: LSV curves of NiO at 1 and 1000 cycles. ....	46
Figure 3.23: LSV curves of S-NiO at 1 and 1000 cycles.....	46
Figure 3.24: LSV curves of Co <sub>3</sub> O <sub>4</sub> at 1 and 1000 cycles. ....	47
Figure 3.25: LSV curves of S-Co <sub>3</sub> O <sub>4</sub> at 1 and 1000 cycles.....	47
Figure 3.26: LSV curves of NiO-Co <sub>3</sub> O <sub>4</sub> at 1 and 1000 cycles.....	48
Figure 3.27: LSV curves of S-NiO-Co <sub>3</sub> O <sub>4</sub> at 1 and 1000 cycles.....	48
Figure 3.28: LSV curves of PAN at 1 and 1000 cycles. ....	49
Figure 3.29: LSV curves of S-PAN at 1 and 1000 cycles. ....	50
Figure 3.30: LSV curves of NiO at 1 and 1000 cycles.....	50
Figure 3.31: LSV curves of S-NiO at 1 and 1000 cycles.....	51
Figure 3.32: LSV curves of Co <sub>3</sub> O <sub>4</sub> at 1 and 1000 cycles.....	51

Figure 3.33: LSV curves of S-Co <sub>3</sub> O <sub>4</sub> at 1 and 1000 cycles. ....	52
Figure 3.34: LSV curves of NiO-Co <sub>3</sub> O <sub>4</sub> at 1 and 1000 cycles.....	52
Figure 3.35: LSV curves of S-NiO-Co <sub>3</sub> O <sub>4</sub> at 1 and 1000 cycles. ....	53
Figure 3.36: OER Tafel plots of PAN, NiO, Co <sub>3</sub> O <sub>4</sub> , and NiO-Co <sub>3</sub> O <sub>4</sub> samples .....	54
Figure 3.37: OER Tafel plots of S-PAN, S-NiO, S-Co <sub>3</sub> O <sub>4</sub> , and S-NiO-Co <sub>3</sub> O <sub>4</sub> samples. ....	54
Figure 3.38: Zim versus Zre of PAN at different potentials .....	55
Figure 3.39: Zim versus Zre of S-PAN at different potentials .....	55
Figure 3.40: Zim versus Zre of NiO at different potentials .....	56
Figure 3.41: Zim versus Zre of S- NiO at different potentials.....	56
Figure 3.42: Zim versus Zre of Co <sub>3</sub> O <sub>4</sub> at different potentials .....	57
Figure 3.43: Zim versus Zre of S-Co <sub>3</sub> O <sub>4</sub> at different potentials .....	57
Figure 3.44: Zim versus Zre of NiO-Co <sub>3</sub> O <sub>4</sub> at different potentials.....	58
Figure 3.45: Zim versus Zre of S-NiO-Co <sub>3</sub> O <sub>4</sub> at different potentials .....	58
Figure 3.46: SEM image of PAN.....	60
Figure 3.47: SEM image of PAN.....	60
Figure 3.48: SEM image of S-PAN .....	61
Figure 3.49: SEM image of S-PAN .....	61
Figure 3.50: SEM image of NiO.....	62
Figure 3.51: SEM image of NiO.....	62
Figure 3.52: SEM image of S-NiO .....	63
Figure 5.53: SEM image of S-NiO .....	63
Figure 3.54: SEM image of Co <sub>3</sub> O <sub>4</sub> .....	64
Figure 3.55: SEM image of Co <sub>3</sub> O <sub>4</sub> .....	64
Figure 3.56: SEM image of S-Co <sub>3</sub> O <sub>4</sub> .....	65
Figure 3.57: SEM image of S-Co <sub>3</sub> O <sub>4</sub> .....	65
Figure 3.58: SEM image of NiO-Co <sub>3</sub> O <sub>4</sub> .....	66
Figure 3.59: SEM image of NiO-Co <sub>3</sub> O <sub>4</sub> .....	66
Figure 3.60: SEM image of S-NiO-Co <sub>3</sub> O <sub>4</sub> .....	67
Figure 3.61: SEM image of S-NiO-Co <sub>3</sub> O <sub>4</sub> .....	67
Figure 3.62: CA plot of PAN for 16 hours .....	68
Figure 3.63: CA plot of S-PAN for 16 hours.....	68
Figure 3.64: CA plot of NiO for 16 hours .....	69
Figure 3.65: CA plot of S-NiO for 16 hours.....	69
Figure 3.66: CA plot of Co <sub>3</sub> O <sub>4</sub> for 16 hours .....	70
Figure 3.67: CA plot of S-Co <sub>3</sub> O <sub>4</sub> for 16 hours.....	70
Figure 3.68: CA plot of NiO-Co <sub>3</sub> O <sub>4</sub> for 16 hours.....	71
Figure 3.69: CA plot of S-NiO-Co <sub>3</sub> O <sub>4</sub> for 16 hours .....	71
Figure 3.70: Number of cycle versus capacitance retention of PAN.....	72
Figure 3.71: Number of cycle versus capacitance retention S-PAN .....	73
Figure 3.72: Number of cycle versus capacitance retention of NiO.....	73
Figure 3.73: Number of cycle versus capacitance retention of S-NiO .....	74
Figure 3.74: Number of cycle versus capacitance retention of Co <sub>3</sub> O <sub>4</sub> .....	74
Figure 3.75: Number of cycle versus capacitance retention of S-Co <sub>3</sub> O <sub>4</sub> .....	75
Figure 3.76: Number of cycle versus capacitance retention of NiO-Co <sub>3</sub> O <sub>4</sub> .....	75
Figure 3.77: Number of cycle versus capacitance retention S-NiO-Co <sub>3</sub> O <sub>4</sub> .....	76

# **CHAPTER I**

## **INTRODUCTION**

### **1.1 Introduction**

In the past few years, the energy crisis has become one of the major issues for mankind. The rapid economic growth worldwide resulted in significant increase in pollution levels, with the constant increment in the consumption of the fossil fuels, elevating the energy shortage issues in between consumption and wasting. These problems led to great stress to increase as well as promote the development of cleaner and greener energy sources which are more sustainable as well as more efficient, as compared to the present technologies. According to the current estimates, per day consumption of energy worldwide exceeded one million tera joules. Major reasons for higher consumptions of energy include rapid growth in human population across the world and rapid pace of industrialization in developing countries. One other major issue is that source of production for approximately half of the above-mentioned produced energy is fossil fuel which is non-renewable and is responsible for posing negative impacts on the environment such as global warming, toxic emissions and acid rain. Since it is non-renewable form of energy, fossil fuel has limited supply. According to global estimates, approximately one hundred and thirty-five billion tons of crude oil has already been

utilized to power vehicles [1]. Increment in the energy demand on global scale resulted in the increase in prices for energy supply. It has been predicted by many field experts that the prices will increase dramatically in the near future. Hence due to the increasing role of energy in our everyday life, scarcity is expected to occur, posing drastic impacts on the life of individuals as well as society. All these issues suggest that we adopt the best alternative which is to shift to renewable energy sources. The economic growth and continuous improvements in the existing technologies have made conventional sources of energy supply insufficient to meet the energy demands of the world. Recent advancements in different technological fields have been going hand-in-hand along with the increment in the consumption of energy. This problem has emphasized research to develop some efficient energy solutions for the sake of meeting the global demands of energy. Contrary to it, currently available resources of the fossil fuels are depleting at a rapid rate. For tackling this problem, researchers are currently working on the development of cleaner and renewable energy resources, e.g., solar energy, tidal or wind energy. The storage of these energies is itself a difficult task. For this reason, in recent times, significant research has been carried out on the other technologies such as fuel cells, ionic batteries, electrochemical/ supercapacitors etc. [2]. Supercapacitors have shown rapid charging/ discharging potential with longer life cycle as compared to the batteries. Due to this reason, supercapacitors have become a more appealing material for the storage of energy. The applications of this material have also been enhanced and it is now-a-days used in electric vehicles, and other remotely deployed equipment [3].

## **1.2 Renewable Energy Sources**

The renewable forms of energy have gained much interest of the researchers in recent years. Some of these include wind energy, solar energy, geothermal energy, fuel cells etc. The detailed description of each of these technologies is given below.

### **1.2.1 Wind Energy**

It is the energy possessed by wind. A turbine is installed at a certain height. When wind strikes the installed blades of the turbine, the shaft is rotated. This rotation of the shaft results in the spinning of a generator installed along with the strong magnets and as a result energy is produced. In this process, kinetic energy is produced initially through the rotation of blades. This energy is later converted into mechanical energy.

There are two main types of wind turbines. Horizontal axis wind turbine (HAWT) and Vertical axis wind turbine (VAWT) are two types of wind turbines commonly used. The size of the turbine differs widely. The amount of energy which can be generated by any wind turbine mainly depends upon the size of the blades of the wind turbine. However, the small-scale wind turbine can generate 10 kilo watts of electricity. This amount of energy is enough to light a single house. In contrast, large scale wind turbines have a potential to generate electricity up to 10 megawatts. For the development of grid stations, wind farms and power plants, these large-scale wind turbines are often grouped together.

### **1.2.2 Hydropower Energy**

It is the form of energy obtained by the help of water moving with the higher flow. The energy possessed by the moving water is utilized to produce electrical energy by the help of water falling on an installed turbine, from a specific height and pressure. The speed of

the water flow helps to rotate the blades attached to the generator. This rotation causes spinning of the generator, which eventually results in the generation of electrical energy.

### **1.2.3 Geothermal Energy**

Energy produced by the heat in the depth of earth is known as geothermal energy. The presence of high pressure and temperature in the depth of the earth is used for the generation of steam. As a result of high temperature and pressure in the interior of the earth, superheated water in the form of steam is generated. This steam can be harnessed by drilling through the earth and can be used to generate electricity by rotating turbines which in turn spin generators. The heat drawn from the interior of the earth can also be used directly for heating households.

### **1.2.4 Solar Energy**

Solar energy is used extensively for the generation of energy and for supplying the electricity to far off places especially to the places where direct and easy access is not available. Recently, large attention is gained by the photovoltaic cells. These cells are utilized for the conversion of solar energy into electrical energy. Three generations of these cells have been developed by the researchers based on the materials used for their manufacturing.

The first generation of these solar cells were the earliest and were manufactured using silicon. The photovoltaic cells produced in the second generation had comparatively smaller size as compared to the solar cells of the first generation. Moreover, they were prepared in the form of thin layer containing the semi-conductor materials. They were therefore named after their appearance, i.e., thin filmed solar cells. These cells also had an advantage of low costs because less material was utilized in their manufacturing. Then

comes the third generation of photovoltaic cells. These cells were manufactured from novel materials such as dye-sensitized, nano crystal, and polymer-based solar cells. These cells reported to have very high efficiency as well as low cost as compared to the first two generation of photovoltaic cells [7].

### **1.3 Energy Storage Devices**

The energy which is produced by the action of these cells can be stored for future use, if required. Various devices are used for the storage of energy produced by photovoltaic cells. Some of the examples include capacitors, batteries, fuel cells etc. These devices are described below in detail.

#### **1.3.1 Battery**

A battery is the simplest device for energy storage. The energy is produced in a battery by the help of chemical reactions as soon as the other components of the circuit are allowed to pass on their electrons in the external circuit attached to the battery. Batteries are mainly divided into two types, i.e., primary batteries and secondary batteries.

The category of primary battery includes only those batteries which can be used for single time. When it is consumed, all the stored charge is exhausted and then it is disposed of. One of the commonly used primary battery is the alkaline battery used in various electrical and electronic appliances.

However, secondary batteries can be recharged by the application of current from any suitable external source, if the charge is completely consumed. Hence, this type of battery is also known as rechargeable battery. Such batteries are mostly used in vehicles and other large-sized machines.

### 1.3.2 Fuel Cell

The fuel cell is one of the latest invented energy systems. Much research is being carried out on this system, in present times. In this system, the chemical energy possessed by the hydrogen is converted into the electrical energy. This hydrogen can be utilized to produce clean energy for lighting homes, public places such as hospitals and offices, hence, minimizing the dependency of these buildings on the national grid systems. **Figure 1.1** shows a typical fuel cell and its working mechanism.

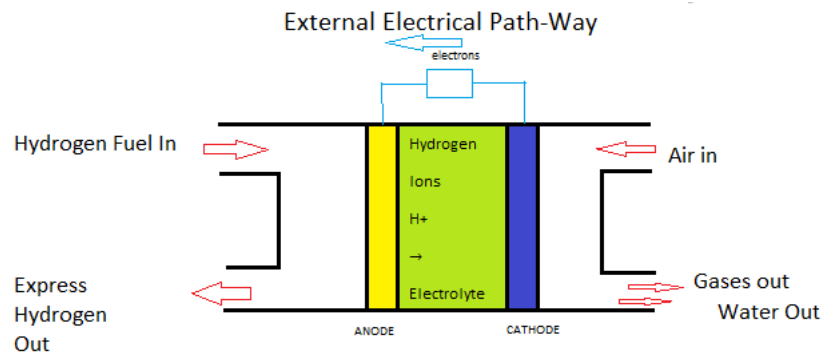


Figure 1.1: Fuel cell

In fuel cells, supply of raw materials for the reactions is needed on a continuous basis. The flow of electrons is assured by the occurrence of an electrochemical reaction taking place between the hydrogen and oxygen. Electrical energy is generated because of the passage of electrons from one electrode to another. These systems also have external storages for storing the reactants. Moreover, the occurrence of reaction can result in the generation of energy and heat as well as water.

A major difference between a battery and a fuel cell is that a fuel cell behaves like a chemical battery where all the reactants are not present inside it; instead, they come from

external sources. Contrary to it, batteries used to store electrical energy by chemical means inside a closed boundary system.

They have depicted very high efficiency even at higher temperatures. One limitation in these cells is that they usually have very high costs because the metals used as catalysts in these cells are very expensive. In certain conditions, they are used in combination with the supercapacitors and batteries for the provision of high power and energy combinations.

### **1.3.3 Capacitors**

Conventional capacitors are also called condensers. A typical dielectric material is used between the two conducting plates with opposite charges. Commonly used materials for this purpose are glass, specific type of plastics, ceramics etc. An electric field is developed between the plates which is directly proportional to the magnitude of charges present on the plates. Supercapacitors are high-capacity capacitors with capacitance value much higher than other capacitors. Based on working mechanisms, following are the three classes of capacitors, developed by the researchers:

- Electric double layer capacitors (EDLCs)
- Pseudo capacitors [12]
- Hybrid capacitors

#### **1.3.3.1 Electric Double Layer Capacitors**

These capacitors can store the charge by the help of electrostatic interactions. These interactions promote the physical adsorption and desorption of ions on the interface of electrolyte /electrode. During the process of charging and discharging, materials of the

electrode do not take any part in the chemical reaction. The transportation of ions, led by the adsorption phenomenon or the phenomenon of desorption, possibly occurs in a short span of few seconds, providing the ability of easy and fast charging and discharging to the EDLCs. However, the specific capacitance of these supercapacitors is closely linked with the available surface area, pore structure and the distribution of pore size [13]. For this reason, most of the times, carbon containing materials like activated carbon, carbon nanotubes or graphene are utilized [14]. **Figure 1.2** below describes the typical mechanism of EDLCs.

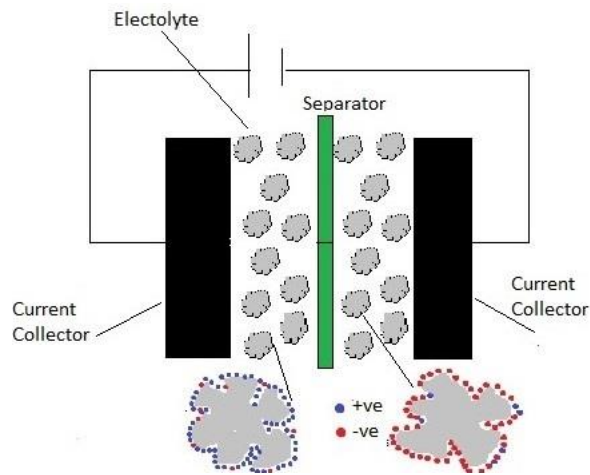


Figure 1.0: Schematic representation of electric double layer capacitors

### 1.3.3.2 Pseudo Capacitors

Pseudo capacitors are used for the storage of energy based on fast as well as easily reversible Faradaic redox reactions. Usually, the specific capacitance of these capacitors is higher than that of EDLCs. The reason behind the higher value is the occurrence of redox reaction of the surface as well as in the electrode materials. However, it results in the lower cyclic stability of Pseudo capacitors [16]. Commonly used polymers for this

purpose include polyaniline (PANI), polypyrrole (PPy), and metal oxides (MnO<sub>2</sub>, NiO, etc.) [17].

### **1.3.3.3 Hybrid Capacitors**

The term hybrid capacitors is used when two electrodes are paired with different charge storage behaviors, one capacitive and one Faradaic, with the performance of such a device in between a supercapacitor and a battery. The main challenge capacitors is to develop them with high energy density that is close to those current rechargeable batteries, while maintaining their inherent characteristics of high power and long cycling life. As a result, many researchers devoted effort to enhancing their performance by maximizing the specific capacitance (nano-sizing) and increasing the cell voltage (building hybrid supercapacitors). With this effort both the performance of supercapacitors and their corresponding applications are gradually improved.

## **1.4 Materials Used for Energy Application**

Nanomaterials offer high surface area and porosity. Nanomaterials may include different items such as nanofibers, nanowires, nanoplates, quantum dots etc. Nanomaterial is however, defined as any material which exists naturally or is manufactured synthetically and can process the unbound, aggregated or agglomerated particles where the dimensions of these particles lie in the range of 1 to 100 nanometers [19].

### **1.4.1 Types of Nanomaterials**

Nanomaterials can be classified into four major groups, i.e., carbon derived nanomaterials, inorganic nanomaterials, organic nanomaterials, and composite based nanomaterials. The brief description of each of these types is given below.

#### **1.4.1.1 Carbon Derived Nanomaterials**

The backbone of these types of nanomaterials is carbon. These materials can exist in various shapes such as hollow tubes, spherical orientations and in the form of ellipsoids. Some other examples also include fullerenes (C-60), carbon nanotubes (CNTs) and nanofibers, carbon black, graphene, and carbon onions. Commonly used methods to produce nanomaterials include laser ablation technique, arc discharge methodology, and chemical vapor deposition (CVD) process etc. [20].

#### **1.4.1.2 Inorganic Nanomaterials**

The inorganic type of nanomaterials usually includes metals as well as metallic oxides. These materials can be utilized for the synthesis of various materials such as silver-based nanomaterials, titanium-oxide based inorganic nanomaterials and zinc oxide-based inorganic nanomaterials.

#### **1.4.1.3 Organic Nanomaterials**

The organic type of nanomaterials is usually synthesized by the assistance of organic matter, other than carbon containing or inorganic metals containing nanomaterials. These organic nanomaterials can easily be transformed into structures as desired. Common examples include nano-polymers in the form of dendrimers, micelles, liposomes, and polymer. This characteristic is provided by the presence of very weak non-covalent bonds present between the atoms.

#### **1.4.1.4 Composite-based Nanomaterials**

This type of nanomaterials is composed of the multiphase nano-polymers as well as nanomaterials. In such types of nanomaterials, there exists one phase having a dimension in the nanoscale. This phase of the material can however be connected to the other nano-

polymer or nano-polymers attached with large sized bulk materials or highly complex structures like metal-organic frameworks. Moreover, in such cases, we can also use a combination of various materials such as carbon-containing materials, metallic materials, organic type of materials along with any other materials such as metallic, ceramics based, or polymer-based bulk materials.

#### **1.4.2 Division on the Basis of Dimensions**

Nano materials and polymers are utilized extensively in various applications. The first idea for the classification of nanomaterials was by Gleiter et al. [21]. They established a classification system based on their crystalline formations and chemical structure. The only limitation in this system proposed was that it was not complete in all aspects because nano-polymers and nano structured materials were not included in this system [22]. However, in the year 2007, a new classification system was proposed by the two researchers, Pokropivny and Skorokhod. They classified nano materials into 4 different classes which were named as class 0D, 1D, 2D and 3D [23]. This system of classification was primarily based upon the movement of electrons along any specific dimension inside the nanomaterial. For instance, the electrons found inside the 0D nanomaterial were entrapped inside a dimensionless space. However, the electrons present inside the 1D nanomaterials were free to move along the x-axis dimension. In the similar manner, 2D nanomaterials can move in x as well as y-axis directions while 3D nanomaterials are free to move in any of the x, y, and z-axis dimensions. This capability of predicting the properties of nanomaterials was used to identify the classification value of nanomaterials which are under evaluation. In the classification system proposed by Gleiter, the properties of nanomaterials have a close association with the grain boundaries. Then

again, Pokropivny and Skorokhod's classification system suggested that the characteristics/ properties of nanomaterials are affected by properties such as shape of the particle and its dimensionality [23].

### **1.4.3 Division Based on the Origin**

Apart from the above-mentioned methods of classification, researchers have also classified nanomaterials based on their origin. The two classes developed by the researchers in this type of classification are described below.

#### **1.4.3.1 Natural Nanomaterials**

This type of material is produced naturally. The main reasons behind their development in natural environments include activities of biological organisms and human activities. Natural environments promote and ensure the availability of artificial surface accompanied by the exclusive micro as well as nano templates for the technological applications. On the surface of earth, naturally occurring nanomaterials are present everywhere, irrespective of the human and environmental interactions.

Naturally occurring nanomaterials are present in all four major spheres of the earth such as atmosphere. Common examples include complete troposphere. However, the example of nanomaterial occurring naturally in hydrosphere include nanomaterials found inside the oceans, inside lakes, in flowing rivers, in groundwater aquifers, and in hydrothermal vents. Nanomaterials are also present in the lithosphere, which consists of rocks and soils, magma at any specific evolutionary stage and the biosphere, covering different types of microbes and higher scaled organisms, also incorporating the human beings in the group [24].

#### **1.4.3.2 Synthetic Nanomaterials**

These nanomaterials are also named as engineered nanomaterials. These materials are mainly produced by the mechanical actions such as grinding, smoke and exhaust of an automobile engine, or they are developed by various scientific techniques including physical, chemical, biological or hybrid techniques. In recent years, their manufacturing has sought a lot of attention because of their extensive applications in the field of product manufacturing and various industrial applications.

Due to this, various questions have been raised on the safety aspects involved in the production as well as handling and end disposal of these materials. Scientists have also developed various strategies for the forecasting of behaviors as well as the fate of various synthetic nanomaterials in different mediums of the environment. One of the major issues prevailing among the researchers in recent times is that they are not sure about the existing knowledge about the behavior and their interactions with other components of the environment [25].

#### **1.4.4 Use of Nanomaterials**

Various carbon-containing materials have been evaluated for their utilization as electrode materials in supercapacitors. One of these materials used is single-walled carbon nanotube (SWCNT) having a theoretical surface area of  $1300 \text{ m}^2/\text{g}$ . This material also exhibited a good response to be used as a supercapacitor electrode [26]. But a major limitation to its wide range use is the higher cost of production and limited surface area [27]. On the other hand, graphene is found to be a highly promising material to be utilized as a supercapacitor. Graphene has shown a theoretical surface area of  $2630 \text{ m}^2/\text{g}$  of material [28], along with higher value of electrical conductivity, higher potential window,

efficient chemical stability, and excellent flexibility [29]. Various studies have also been conducted on the pseudocapacitive materials for the fabrication of electrodes of supercapacitors. Various other compounds like  $\text{MnO}_2$ ,  $\text{NiCo}_2\text{O}_4$  and  $\text{Ni(OH)}_2$  have also been tested, combining them with graphene oxide [30].

The composite electrodes developed by the combination of these materials have shown excellent capacitance properties, it is believed, because the materials can provide the needed amount of pseudo capacitance whereas the EDL capacitance is provided by the means of higher specific surface area of graphene oxide. Moreover, when these materials are used in combination with each other, their life is also increased. Hence, these materials have attracted many researchers to evaluate their potential for supercapacitor applications [31]. These nano-composite materials have been researched extensively in recent times. The main reason of this attention is the properties of these materials such as melting point, thermal conductivity, electrical conductivity, catalytic behavior, ability to absorb light and ability to scatter light. These properties play an important role in improving the performance of these materials.

## **1.5 Properties of Capacitors**

There are various properties of capacitors that are important to discuss. These properties are discussed below.

### **1.5.1 Specific Capacitance**

The charge stored per unit mass of the active material on the electrode of capacitor is known as a specific capacitance [32]. The specific capacitance of a capacitor can be calculated using the formula given below:

$$C_s = \frac{I\Delta t}{m\Delta t} \dots (1.1)$$

Where,  $C_s$  is the specific capacitance,  $\Delta t$  is the time of discharge,  $m$  is the mass of the active material on electrode &  $I$  represents discharged current.

### 1.5.2 Energy and Power Density

Both of these densities play an important role in evaluating the performance of supercapacitors for their use in real applications. Both properties are determined by the help of cyclic voltammetry (CV) as well as by using the galvanostatic charge discharge (GCD) techniques [33]. The specific energy density of a supercapacitor is given by the following formula

$$E = \frac{1}{2} C_s (\Delta V)^2 \dots (1.2)$$

Moreover, the power density is used to determine the mechanism through which the device transfers the energy per unit mass or volume [33]. The equation used for the calculation of power density is given below

$$P_{max} = \frac{(\Delta V)^2}{4mR_{ESR}} \dots (1.3)$$

The average power density can be determined by the help of the formula given below

$$P_{avg.} = \frac{E}{\Delta t} \dots (1.4)$$

### 1.5.3 Ragone Plot

The Ragone plot is a graph showing power density and the energy density of energy devices. This plot assists in identifying the relation existing between power and density of energy storage [33]. **Figure 1.3** shows Ragone plot for various energy devices.

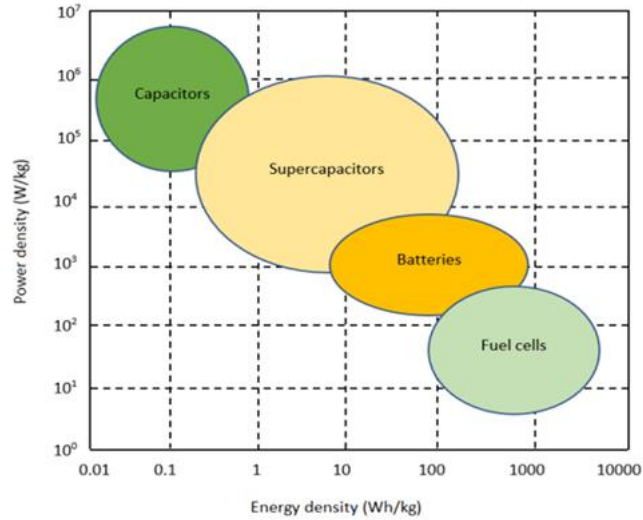


Figure 1.3: Ragone plot for various energy devices

## 1.6 Electrolysis

Electrolysis ensures the provision of a sustainable technology to produce hydrogen and oxygen. Lesser requirements of input materials in the form of water and energy make it a more viable option for the generation of energy [34]. The main limitations in the way of implementing this technology on a larger scale is lower yield. Therefore, there is a need of conducting extensive research on ways through which yield of hydrogen can be increased with higher purity levels [35]. In conventional systems, both gases ( $H_2$  and  $O_2$ ) are produced in the single cell at the same time. These gases can be mixed with each other during electrolysis, causing the degradation of electrolyzes [36]. To overcome this issue, different methods have been devised by various researchers [37].

According to the suggestions made by the Cronin research group [38], a molecular redox mediator material, which is soluble in nature, can be used for the separation of both these gases, produced during common proton exchange membrane-based water electrolysis.

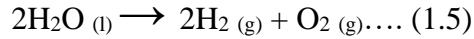
This mediator material assists the electron-coupled exchange of proton that occurs between the O<sub>2</sub> and H<sub>2</sub> evolution reactions [38].

### **1.6.1 Water Splitting Technology**

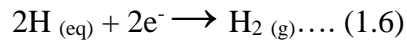
With the increase in energy issues in the world, hydrogen is considered as an efficient and very sustainable source of green energy which can easily serve as an alternative to the energy obtained by the fossil fuel [39]. The reformation of natural gas to produce hydrogen is never recommended as a viable option because large quantities of these non-renewable resources are consumed in the production of hydrogen gas. Moreover, during this process some undesired compounds such as carbon dioxide are also produced which can play a role in increasing the greenhouse effect [40]. Splitting water into hydrogen and oxygen was in practice more than 200 years ago. However, the process is very expensive and there is a need of developing more efficient, green and cost-efficient technology for the production on large scale [41]. Water splitting is a chemical reaction in which water is decomposed into the molecular compounds, i.e., H<sub>2</sub> and O<sub>2</sub> [42]. A potential of electrical energy is normally applied to undergo this separation. This potential is usually higher than the theoretical potential needed for the electrolysis of water to occur [43]. Two types of reactions normally occur. They are

- Oxygen evolution reaction (OER)
- Hydrogen evolution reaction (HER)

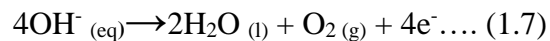
The efficiency of oxygen evolution reaction is higher in an alkaline medium. Alternatively, hydrogen evolution reaction shows higher efficiency in the acidic medium. The reaction that undergoes during water splitting is listed in the form of chemical equation below:



The hydrogen evolution reaction that occurs during the process is shown by the chemical equation given below:



The oxygen evolution reaction that occurs during the process is shown by the chemical equation given below:



### **1.7 Objective of the Thesis**

With the ongoing global energy crisis and environmental concerns, the development of sustainable and renewable energy storage and conversion systems such as electrochemical capacitors, lithium-ion batteries and proton-exchange membrane fuel cells has evolved into an urgent task. Supercapacitors are considered highly complementary to batteries due to their high-power density, extremely long cycle life, low maintenance cost and safe operation. Water electrolysis, among the various alternative energy strategies, constructing an energy infrastructure that uses hydrogen as the primary carrier and connecting a host of energy sources to diverse end uses may enable a secure and clean energy future. To this end, effective storage and production of hydrogen are key elements of the hydrogen economy. Therefore, considering the material properties suitable for the supercapacitors and water electrolysis catalyst electrodes that are efficient and inexpensive to obtain, the main purpose of this thesis is to fabricate nano

fibers and study electrochemical properties of nanofiber. The nanofibers were prepared using PAN as polymer and nickel nitrate and cobalt nitrate as a salt for metal oxides.

## CHAPTER II

### EXPERIMENTAL DETAILS

#### 1.8 Experimental Details

##### 1.8.1 Materials Used

The materials used for the synthesis of nanofibers include N,N-dimethylformamide (DMF), nickel nitrate hexahydrate, polyacrylonitrile and cobalt nitrate hexahydrate.

##### 1.8.2 Preparation of 1D Nanofibers:

1D nanofibers were synthesized in three stages. In the first stage, a homogenous mixture was prepared, followed by the electrospinning of the prepared solution, during the second stage of preparation. In the third and last stage, calcination of the prepared nanofibers was done to produce the 1D nanofibers of metal oxide.

##### 1.8.2.1 First Stage

In the first stage, four different compositions were used to prepare a homogeneous solution for different samples. The first sample was prepared dissolving 0.5 g of polyacrylonitrile in 4.5 g of N,N-dimethylformamide. The second sample was prepared using 0.5 g of polyacrylonitrile in 4.5 g of N,N-dimethylformamide with 1 mol of  $\text{Ni}(\text{NO}_3)_2 \cdot 6\text{H}_2\text{O}$ . The third sample was prepared using 0.5 g of polyacrylonitrile in 4.5 g of N,N-dimethylformamide (DMF) with 1 mol of  $\text{Co}(\text{NO}_3)_2 \cdot 6\text{H}_2\text{O}$ . The fourth sample was prepared using 0.5 g of polyacrylonitrile in 4.5g of N, N-dimethylformamide with 2

mol of  $\text{Co}(\text{NO}_3)_2 \cdot 6\text{H}_2\text{O}$  and 1 mol of  $\text{Ni}(\text{NO}_3)_2 \cdot 6\text{H}_2\text{O}$ . After combining the compositions the samples were mixed for 24 hour utilizing magnetic stirrer. **Figure 2.1** shows the materials used to create homogeneous mixtures.

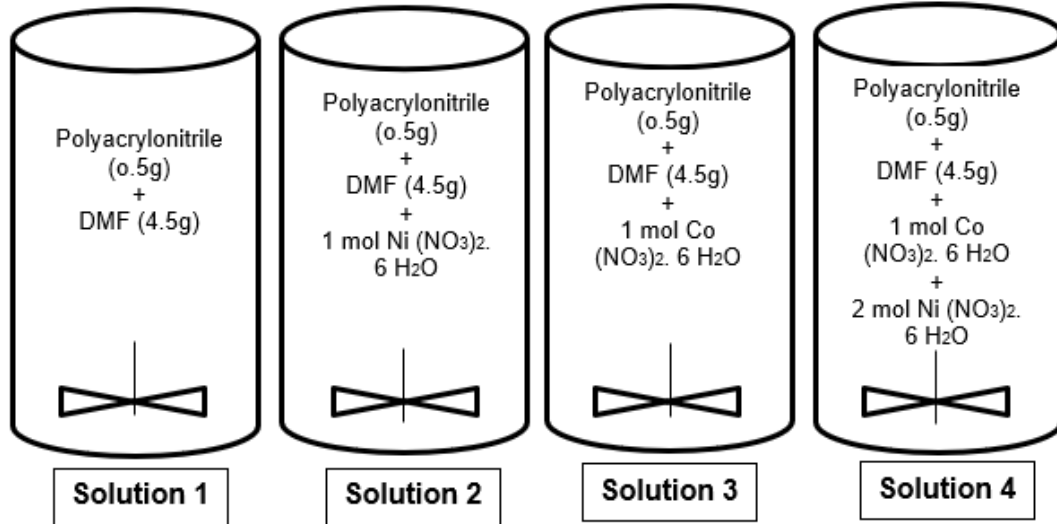


Figure 0.1: Four different compositions used to prepare homogeneous solutions for different samples

### 1.8.2.2 Second Stage

The second stage process involved electrospinning of the homogeneous solution prepared in the first step. Electrospinning is a technique to produce fibers in the range of nanometer to few microns by applying high voltage. The **Figure 2.2** further elaborates the process.

This process involves three main parts: voltage supply, syringe pumping and a fiber collector. The homogeneous solution prepared in the first stage was filled in to a syringe and pumped at constant rate. A charge is usually produced by the application of high potential of between the polymer solution inside the syringe and a collector. An

elongation takes place which gives a conical shape to the droplets, as soon as the critical voltage level is achieved. However, as soon as the value of applied voltage increases from the value of critical voltage, surface tension of the solution is overcome by the electric force of the charged polymer. As a result, an extremely fine and charged jet of solution is emitted from the tip of the syringe. As the jet moves in the air, in the direction of the grounded collector, and its speed of propagation is increased, the solvent is evaporated. Hence, the continuous fibers are obtained on the surface of the grounded collector in the form of a non-woven fabric mat.

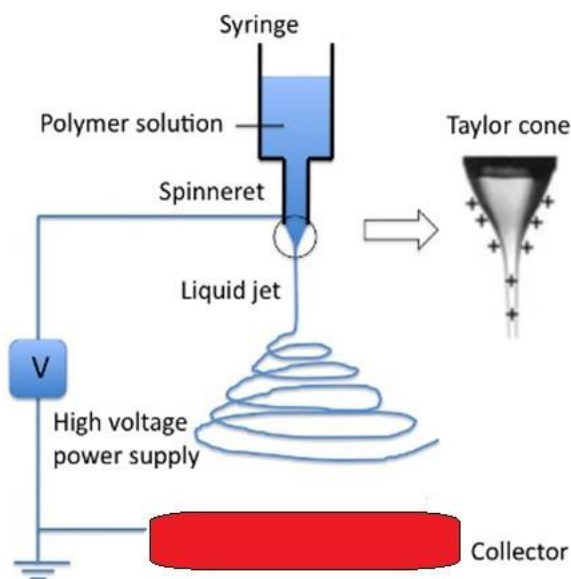


Figure 0.2: Electrospinning process

The flow rate of the solution is controlled by a syringe pump. All samples are electro spun at 0.7 mm/h feed rate and 12 kV. After electrospinning, thermal treatments are necessary to convert into conductive carbon and more activation is needed to prepare high surface area carbon out of the fiber.

### 1.8.2.3 Third Stage

It is the final stage which involves calcine the fibers made from using the electrospun process. PAN is well known for carbon fiber and electrode materials for preparing supercapacitors because of their high thermal stability, mechanical properties and high surface area. This stage involves two steps. The first step is the oxidative stabilization treatment at 250 °C under air which increases the carbon yield and make the structure stable. In this step PAN undergoes cyclization to form stable ladder structure by cross-linking of oxygen molecules. The second step involves carbonization treatment where material is heated at 800 °C under nitrogen gas for 4 hours. This step removes non-carbon elements and improves the electric conductivity. The process is further elaborated with

**Figure 2.3.**

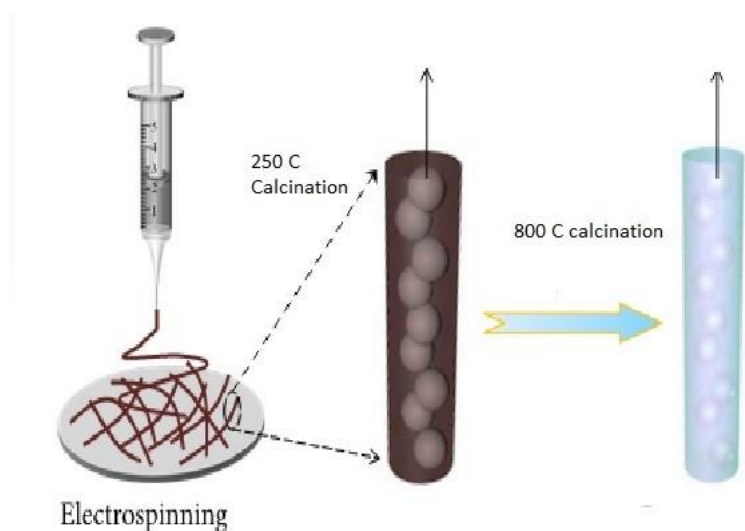


Figure 0.3: Electrospinning and calcination

### 1.8.3 Sulfurization

The sulfurization process was done using 800 mg of sodium sulfide nonahydrate. In typical synthesis, sodium sulfide nonahydrate was dissolved in deionized water with the

help of sonication. After dissolving completely, the measured amount of sample was added and sonicated again to make a homogeneous solution. Then the mixed solution was transferred to a Teflon-lined stainless steel autoclave and heated at 180 °C for 24 h. The reactor cooled to room temperature naturally. The precipitate at the bottom of container was filtered out and washed several times with DI water.

#### 1.8.4 Ni Foam Preparation

Ni foam was cut into proper dimension, then immersed and sonicated in 3M HCl solution for 10 minutes, ensuring the removal of the surface oxide layer. After the successful removal of the oxide layer, the Ni foam was washed and cleaned by using deionized water as well as ethanol. Then the foam was dried and kept in a vacuum oven for 30 minutes at 50 °C

#### 1.8.5 Electrode Making

The solution preparation for electrode was done by using synthesized material shown in **Table 2.1**, PVDF binder and carbon black with ratio of 8:1:1 respectively. That solution was applied to Ni foam and kept it in oven for 48 hours at 60 °C.

Table 0.1: Experimental details for the synthesis of nanofibers

Sample Code	PAN (g)	DMF (g)	NiO (mol)	Co <sub>3</sub> O <sub>4</sub> (mol)	Temperature ( °C)	Sulfurized
PAN	0.5	4.5	0	0	800	N
PAN-NiO	0.5	4.5	1	0	800	N
PAN-Co <sub>3</sub> O <sub>4</sub>	0.5	4.5	0	1	800	N

PAN-Ni-Co <sub>3</sub> O <sub>4</sub>	0.5	4.5	1	2	800	N
S-PAN	0.5	4.5	0	0	800	Y
S-PAN-NiO	0.5	4.5	1	0	800	Y
S-PAN-Co <sub>3</sub> O <sub>4</sub>	0.5	4.5	0	1	800	Y
S-PAN-NiO-Co <sub>3</sub> O <sub>4</sub>	0.5	4.5	1	2	800	Y

### 1.8.6 Electrochemical Measurements

The main purpose of the experiment is to study the electrochemical performance of eight samples as shown in **Table 2.1**, for supercapacitor and catalysts. All the electrochemical tests were performed at room temperature using a three-electrode system. The three-electrode cell system has three different electrodes. A platinum wire as a counter electrode, a saturated calomel and Hg/ HgO electrodes as reference electrodes, and as-synthesized nanofibers on nickel foam as a working electrode. All electrochemical tests were conducted using VersaStat 4-500.

The electrochemical performance of these samples was tested for supercapacitor application via cyclic voltammetry, galvanostatic charge-discharge measurements, and electrochemical impedance spectroscopy.

Oxygen evolution and hydrogen evolution reactions of these samples were tested for fuel cell application. The linear sweep voltammetry, chronoamperometry, and electrochemical impedance spectroscopy were performed to study electrocatalyst properties and potentials toward OER and HER. The techniques used for these measurements are elaborated further.

### 1.8.6.1 Cyclic Voltammetry

It is considered as one of the powerful electrochemical techniques usually implemented for the investigation of reduction as well as oxidation reaction processes among the molecular species. **Figure 2.4** below describes a typical voltammogram used to describe the cyclic voltammetry profile of a material.

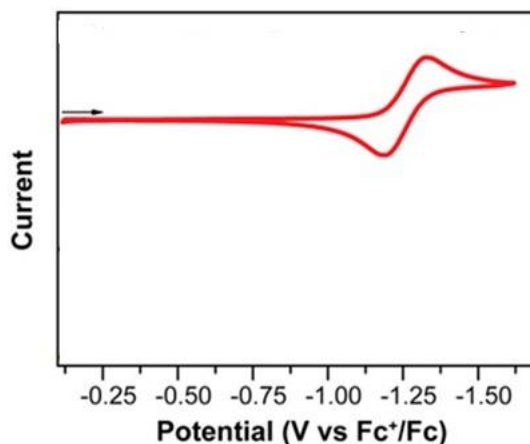


Figure 0.4: Cyclic voltammogram

In these types of profiles, the parameter which is imposed on the system is plotted on the x-axis. For example, in **Figure 2.4** the imposed parameter is the potential applied (E). On the other hand, the response is recorded on the y-axis. For example, in the above **Figure 2.4**, the response is current (i) passed through the material.

The arrow represents the direction in which potential was applied during the data collection phase. The arrow represents the direction of initiation as well as sweep direction for the first segment.

### 1.8.6.2 Electrochemical Impedance Spectroscopy

It is an electrochemical technique which is extensively used for the measurement of impedance of any system which depends upon the AC potentials frequency. The method has gained importance in recent years. One of the main reasons behind this is that this method is capable of separating of the impacts of various components which means the role played by the electron transfer resistance, double layer capacity etc. **Figure 2.5** shows a typical electrochemical impedance spectroscopy system

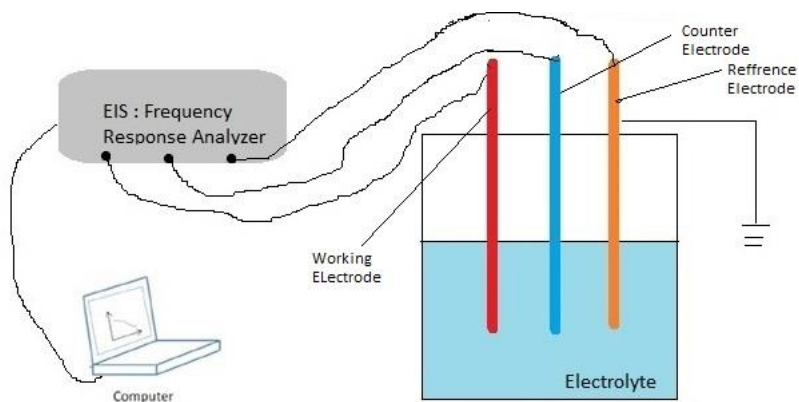


Figure 0.5: Three electrode test

### 1.8.6.3 Linear Sweep Voltammetry

In this type of technique, a fixed potential range is applied much like the potentiostat measurement. But the applied voltage is usually scanned from low to high limit as represented in **Figure 2.6**.

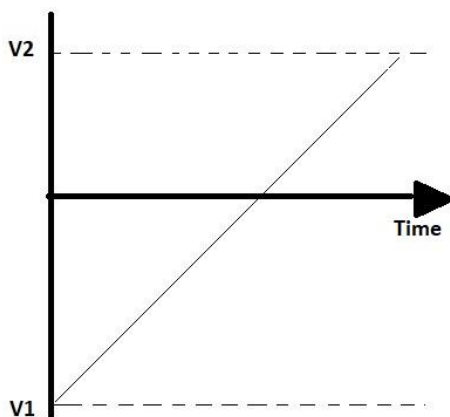


Figure 0.6: Linear sweep voltammetry

The scan rate can be changed by varying the time consumed for sweeping the range.

The characteristics of the voltammogram depends upon different factors such as

- The rate of electron transfer reaction
- Voltage scan rate
- Chemical reactivity of electroactive species

#### 1.8.6.4 Chronoamperometry

This is a technique which depends upon the time and a square-wave potential which is applied to a working electrode. Chronoamperometry is used to study the kinetics of chemical reactions, diffusion processes, and adsorption. In this technique, a potential step is applied to the electrode and the resulting current vs. time is observed.

#### 1.8.7 Tafel Slope

Tafel analysis is a promising technique utilized extensively for the comparison of electrocatalytic activities as well as for the demonstration of the mechanism of the reaction that occurs during electrocatalysis. During the application of this technique, the

sensitivity of the electric current response to the applied potential in the form of Tafel slope is identified.

The result of developed slope provides fruitful information that can be used for the determination of the rate steps of the reaction. Moreover, that can also utilize the experimentally obtained results with the theoretical results considering various rate determining steps which are primarily based on the microkinetic model.

### **1.8.8 Electrochemical Stability Test**

This is one of the most important parameters for the commercial use of electrochemical catalysis. There are two methods to measure catalyst stability. The first method is the constant current or potential method that involves carrying out long-term catalytic reaction of the electrolysis device under given current or voltage and analyzing the duration of non-decay. The second method for measuring involves cyclic voltammetry, in which thousands of cyclic scans are performed to observe changes in the polarization curve before and after the cycle to determine the performance of the catalyst.

## CHAPTER III

### RESULT AND DISCUSSION

#### 1.9 Result and Discussion

The results of the analysis are discussed in detail below.

##### 1.9.1 Cyclic Voltammetry

Cyclic voltammetry and galvanostatic charge-discharge measurements were performed to study the electrochemical properties of different electrodes. The effects posed by different materials such as nickel oxide, cobalt oxide and sulfides on the electrochemical properties were investigated. Cyclic voltammograms of samples with sulfurized and un-sulfurized were compared (**Figure 3.1** to **Figure 3.8**). For typical cycle voltammograms, the CV curves usually show one redox peak for the samples with one oxidation and reduction process. These peaks reveal the electrodes behavior while storing charge, attributed to the faradic type's reversible redox reactions.

A study of the CV curves revealed that, while increasing the scan rates from 2 -300 mV/s, the peak shifts to higher potential throughout the oxidation process and a lower during reduction. The redox behavior can be found in all the given cyclic voltammograms of evaluated samples. This shows that one of the predominant methods for the storage of energy in this system is the redox process. It is very important to note that the CV curves should have a rectangular shape for the EDLC's.

The shape and nature of the cyclic voltammograms of the synthesized samples suggest that the capacitance is mainly due to pseudo-capacitance.

The specific capacitance of each electrode is obtained using CV measurements, using the following equation

$$C_{sp} = \frac{Q}{\Delta V \times \left(\frac{\partial V}{\partial t}\right) \times m} \dots (3.1)$$

Where,  $m$  is the mass of the electrode material,  $Q$  is the total area bound by the curve in millicoulombs,  $V$  is the difference between the maximum and minimum potential difference in volts (V),  $\left(\frac{\partial V}{\partial t}\right)$  is the scan rate.

When a graph of specific capacitance against scan rate is plotted (**Figure 3.9**), it shows proportionality between the two; that is, an increase in the scan rate results in a decrease in specific capacitance. This trend might be attributed to an insufficient time during which the redox reaction is supposed to occur. The concentration of ions at the electrode's active zone grows so immensely that the electrolyte diffusion rate will not be sufficient to allow the electrochemical reactions to occur.

It was observed the peak position shifts towards higher potential during the oxidation process and lower potential during the reduction process upon increasing scan rate from 2 – 300 mV/s. **Figure 3.1** shows the CV graph of PAN. It show the oxidation peak at 0.47 V at scan rate of 2 mV/s, which shifted to 0.49 V at 10 mV/s. **Figure 3.2** shows the CV curve of the sulfurized PAN, sulfurization of the PAN shifted oxidation peak from 0.49 V to 0.54 V at 10 mV/s. Sulfurization has improved integral area of the curve, which means it can store more charges. **Figure 3.3** shows the CV of nickel oxide sample and **Figure 3.5** shows the CV of the cobalt oxide sample, both graphs show the great amount

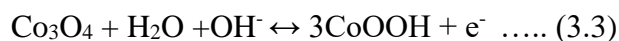
of increase in the integral area of the curves. Inclusion of the transition metals has significantly increased the charge storage capacity. The nickel oxide sample shows a good amount of charge storing capacity. **Figure 3.4** and **Figure 3.6** shows the sulfurized nickel oxide and cobalt oxide samples CV respectively. The presence of sulfur shown in the huge amount of increase in charge storing capacity for the NiO sample where for the Co<sub>3</sub>O<sub>4</sub> sample it shows little amount of increase in charge storage capacity. **Figure 3.7** shows the CV of nickel oxide and cobalt oxide mixed sample at a scan rate from 2 – 300 mV/s. All curves exhibit a pair of well-defined redox peaks, corresponding to the faradic reaction. One pair of redox peaks in CV is observed due to the good mixing of NiO and Co<sub>3</sub>O<sub>4</sub> ions. NiO-Co<sub>3</sub>O<sub>4</sub> sample shows the oxidation peak at 0.51 V at 300 mV/s scan rate. **Figure 3.8** shows the sulfurized S-NiO-Co<sub>3</sub>O<sub>4</sub>, that shows the peak at 0.5 V at 300 mV/s. It does show the little higher integral area of the curve than the NiO-Co<sub>3</sub>O<sub>4</sub> sample. Redox reactions for the nickel oxides and cobalt oxides shown below:

### **Redox Reactions:**

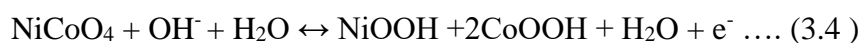
Nickel Oxide



Cobalt Oxide



Nickel- Cobalt Oxide



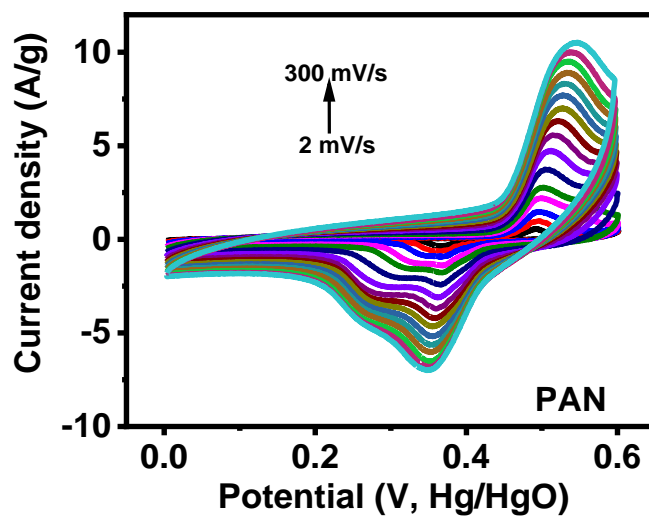


Figure 0.1: CV curves of PAN sample at various scan rates

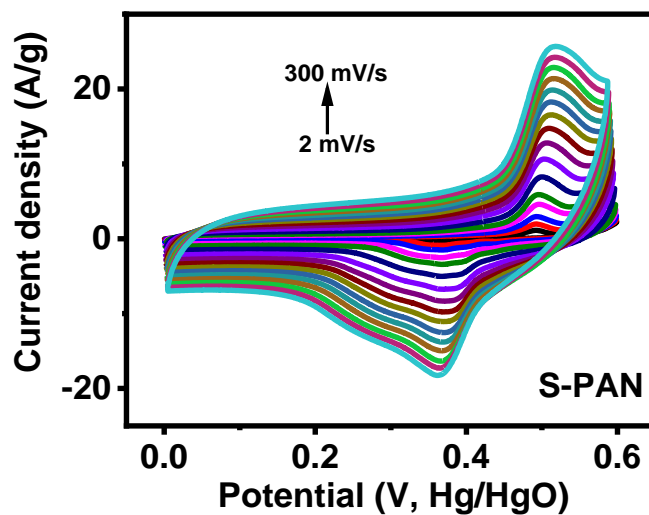


Figure 0.2: CV curves of S-PAN sample at various scan rates

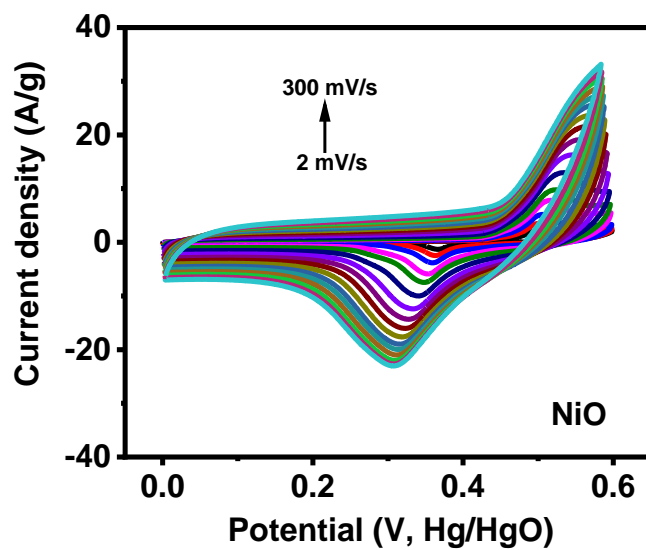


Figure 0.3: CV curves of NiO sample at various scan rates

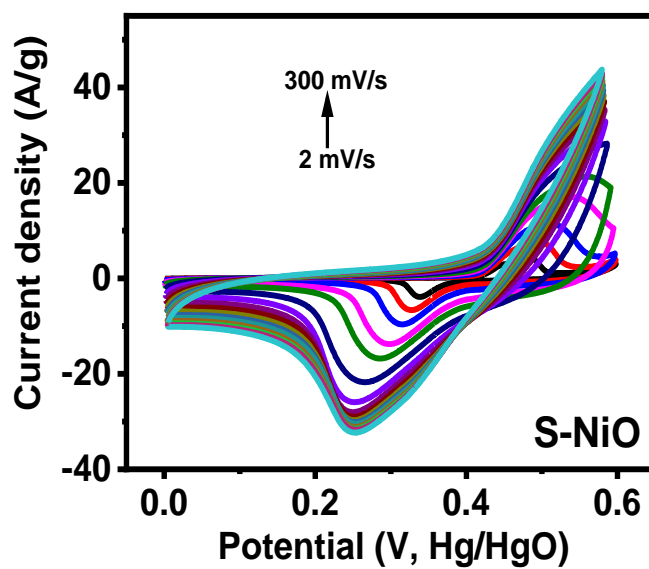


Figure 0.4: CV curves of S-NiO sample at various scan rates

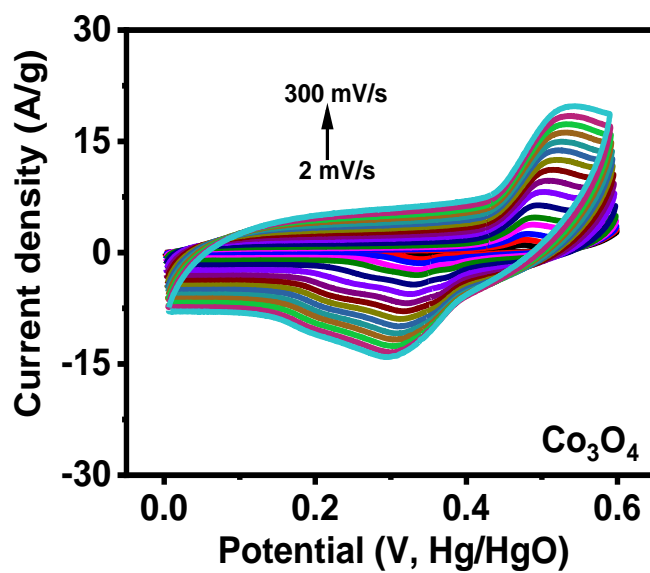


Figure 0.5: CV curves of  $\text{Co}_3\text{O}_4$  sample at various scan rates

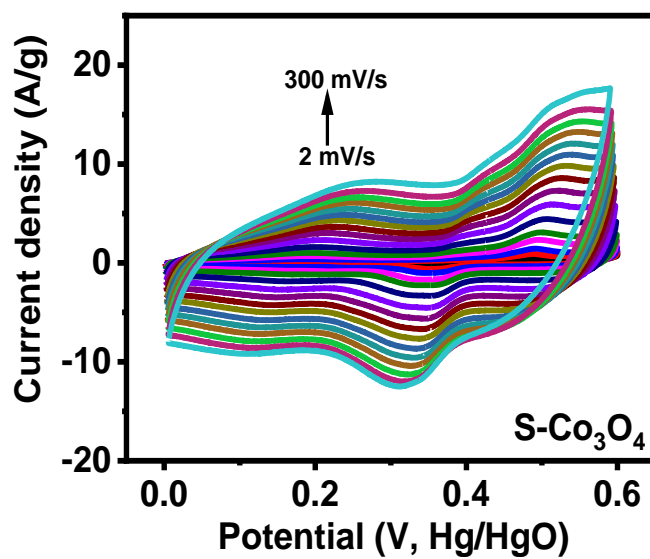


Figure 0.6: CV curves of S- $\text{Co}_3\text{O}_4$  sample at various scan rates

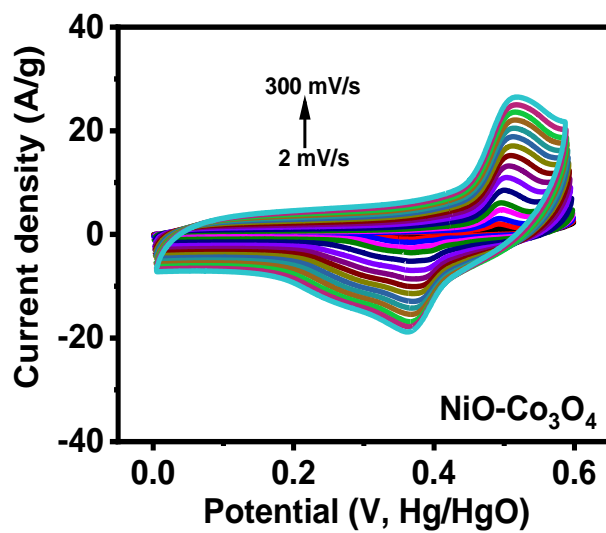


Figure 0.7: CV curves of NiO-Co<sub>3</sub>O<sub>4</sub> sample at various scan rates

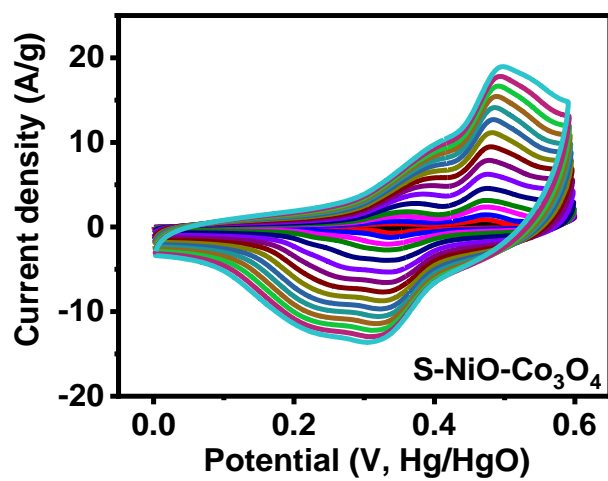


Figure 0.8: CV curves of S-NiO-Co<sub>3</sub>O<sub>4</sub> sample at various scan rates

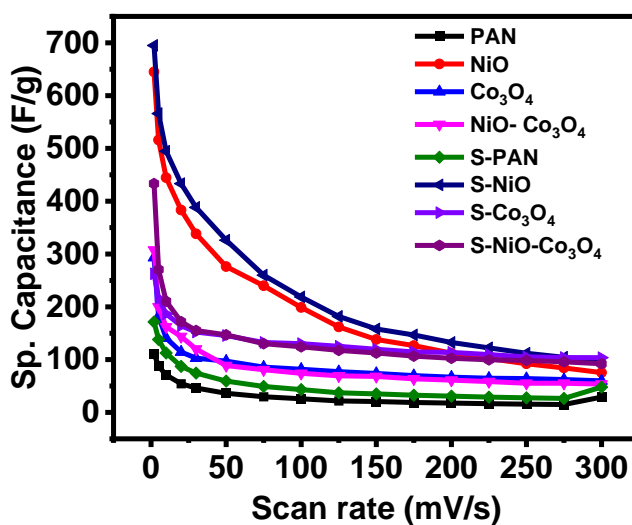


Figure 3.9: Scan rate versus specific capacitance

Table 3.1 Calculated specific capacitance from CV curve

Sample Name	Specific capacitance (F/g)
PAN	111
NiO	644
Co <sub>3</sub> O <sub>4</sub>	293
NiO- Co <sub>3</sub> O <sub>4</sub>	307
S-PAN	171
S-NiO	694
S-Co <sub>3</sub> O <sub>4</sub>	262
S-NiO-Co <sub>3</sub> O <sub>4</sub>	433

### 1.9.2 Galvanostatic Charge-Discharge Analysis

This analysis proved highly efficient in testing the storage capacity of the samples. The investigation revealed that the GCD curves were symmetrical, indicating high reversibility of the tested samples. Also, an increase in current density produced a corresponding decrease in discharge time. This was due to the diffusion effect. This effect tends to limit OH<sup>-</sup> ions within the electrodes upon applying extreme current density.

From the results, it can be determined which samples displayed the longest discharge time, indicating that it has the largest capacitance compared to the other samples. The specific capacitance can also be deciphered from GCD curves as shown in the equation below

$$Cs = \frac{I \times \Delta t}{m \times \Delta V} \dots (3.5)$$

Where, Cs represent the specific capacitance per gram (F/g), I represent the discharging current (mA),  $\Delta t$  is the time the setting takes to discharge in seconds, and m is the mass of material (g), and  $\Delta V$  is the potential window (V).

Comparing the electrodes' GDC curves will confirm that the specific capacitance decreases when the discharge current increases. This decrease can be explained as a result of the increase in the rate of potential difference and the inadequate amount of time allowed by the redox process's reaction to occur at large discharge currents.

**Figure 3.10** reveals the charge-discharge of PAN at different current densities. When the current density is higher than 5 A/g, the charge-discharge curves cannot accurately reflect the properties of PAN. It can be seen from the low current density charge-discharge curve that PAN has obvious electrical double-layer capacitance characteristics, but it has poor performance in constant current charge-discharge tests. **Figure 3.11** shows the charge-discharge curve of sulfurized PAN; it has shown the little improvement in performance of charge-discharge at lower current density. Transition metal oxides (cobalt oxides, nickel oxides) presence takes a longer time to complete the charge-discharge than PAN. This means that specific capacitance of the materials increased. **Figure 3.12** shows the charge-discharge of nickel oxide material which is taking almost three times longer to

finish charge-discharge cycle at lower current densities. The sulfurized nickel oxide sample shows even better specific capacitance. **Figure 3.14** shows the graph for the cobalt oxide sample; it doesn't have as impressive results as nickel oxide. It shows the better results than PAN. The sulfurized cobalt oxide sample (**Figure 3.15**) takes a longer time to finish the charge-discharge cycle than the unsulfurized cobalt oxide. **Figure 3.16** and **Figure 3.17** shows the charge-discharge curve for the NiO-Co<sub>3</sub>O<sub>4</sub> mixture sample and sulfurized NiO-Co<sub>3</sub>O<sub>4</sub> sample, It is clearly showing that sulfurization improved charge storing capacity. It was noteworthy that the charge-discharge time of the all sulfurized material is greatly improved. **Figure 3.18** shows the graph for specific capacitance versus current density for unsulfurized sample and **Figure 3.19** for the sulfurized sample.

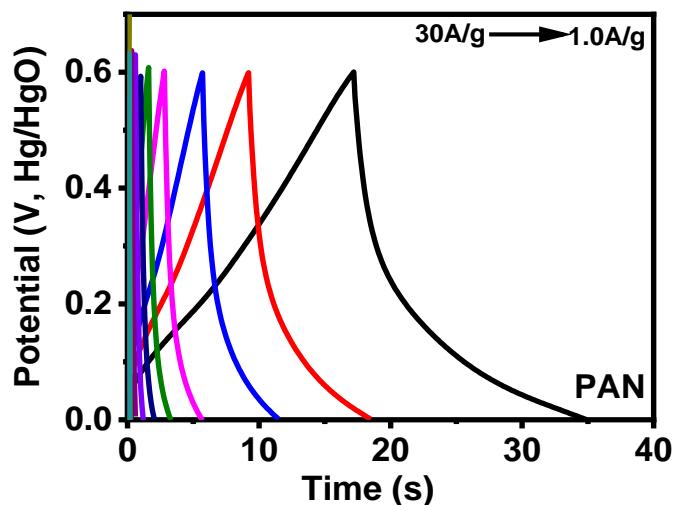


Figure 0.10: Potential versus time at different current density for PAN

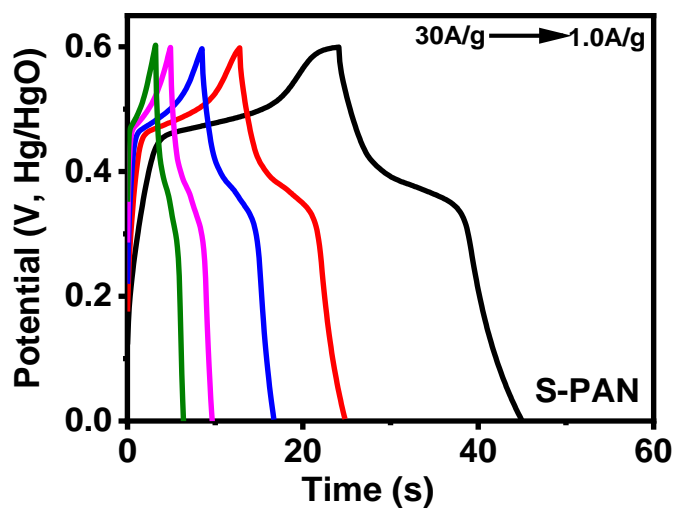


Figure 0.11: Potential versus time at different current density for S-PAN

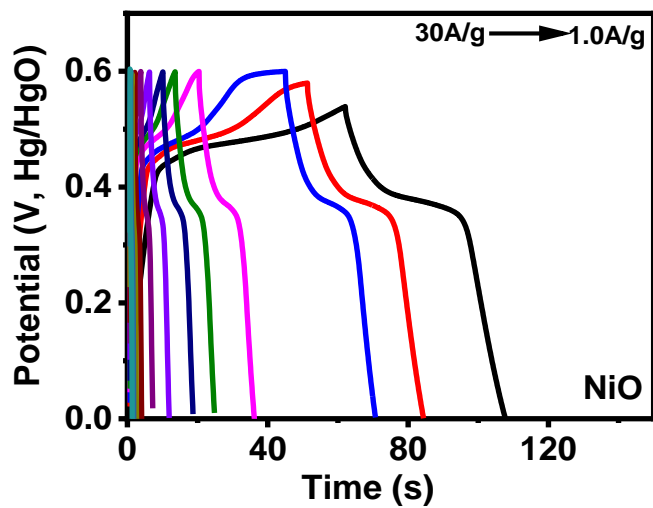


Figure 0.12: Potential versus time at different current density for NiO

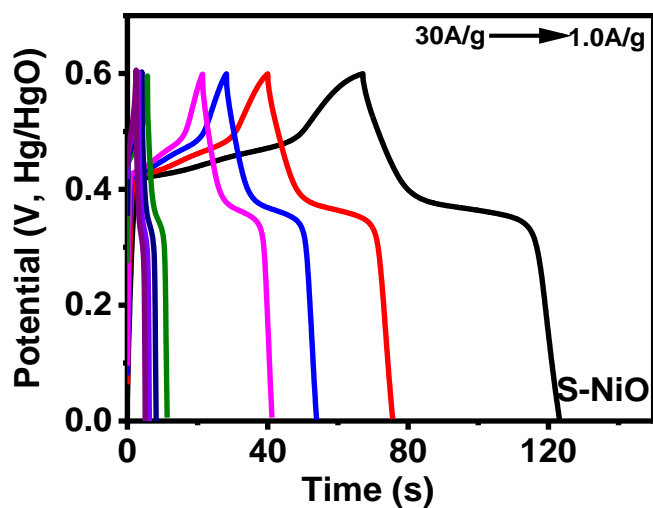


Figure 0.13: Potential versus time at different current density for S-NiO

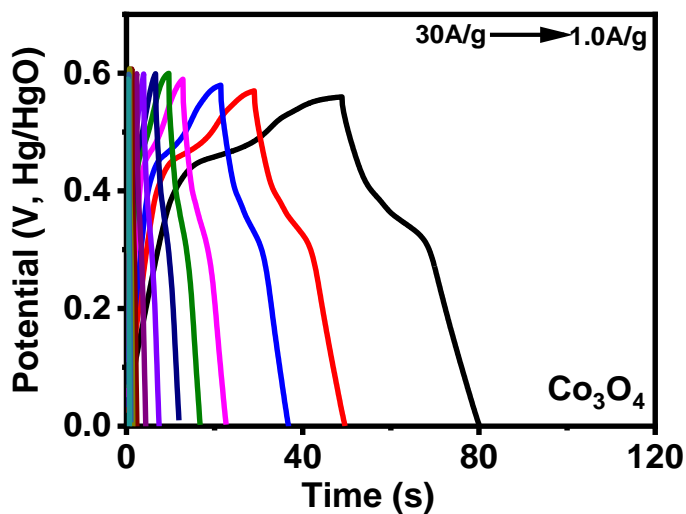


Figure 0.14: Potential versus time at different current density for Co<sub>3</sub>O<sub>4</sub>

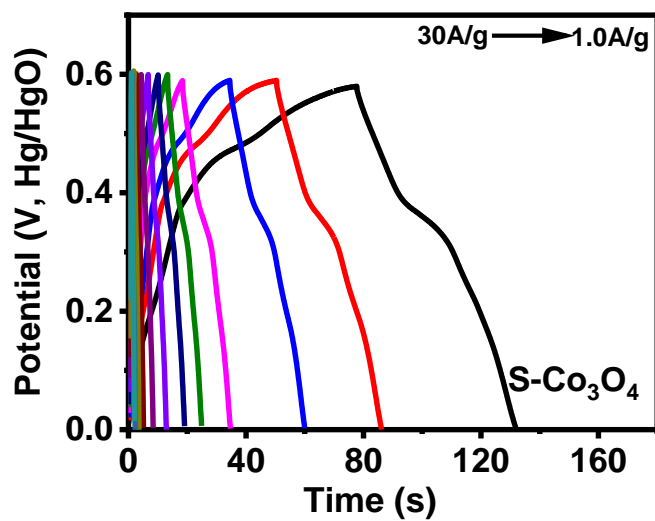


Figure 0.15: Potential versus time at different current density for S-Co<sub>3</sub>O<sub>4</sub>

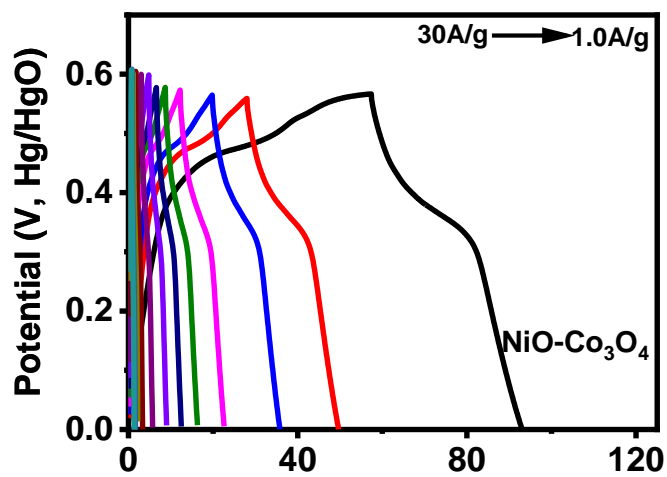


Figure 0.16: Potential versus time at different current density for NiO-Co<sub>3</sub>O<sub>4</sub>

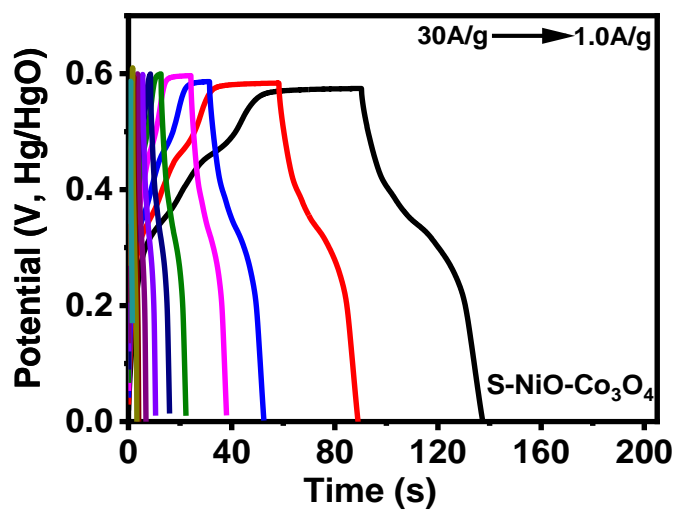


Figure 0.17: Potential versus time at different current density for S-NiO-Co<sub>3</sub>O<sub>4</sub>

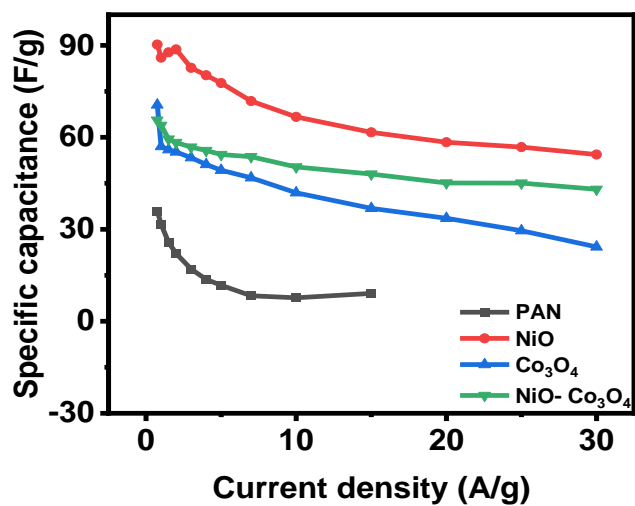


Figure 0.18: Specific capacitance versus current density for unsulfurized sample

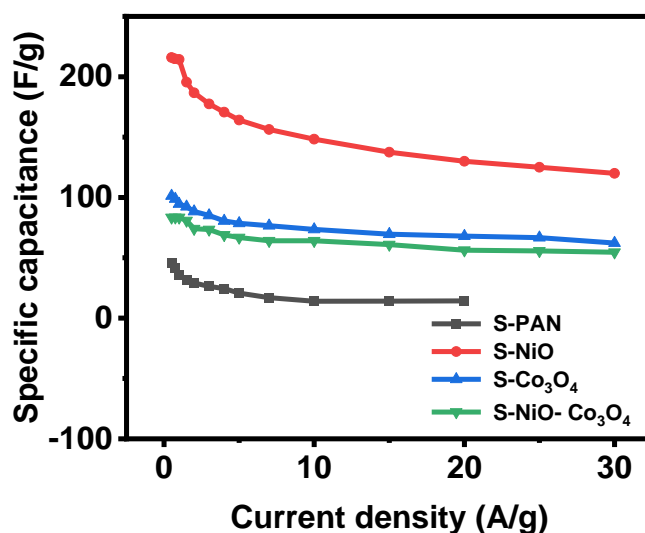


Figure 0.19: Specific capacitance versus current density for sulfurized sample

### 1.9.3 Electrocatalyst for Oxygen Evolution Reaction

An oxygen evolution reaction is the limiting chemical reaction process of producing oxygen, such as the oxidation of water during oxygenic photosynthesis, electrolysis of water into oxygen and hydrogen, and electrocatalytic oxygen evolution from oxide and oxoacids. The performance of samples was investigated in 1M KOH solution in a typical three-electrode set up as previously discussed. The linear sweep voltammetry curve at 2 mV/s scan rate and their respective overpotentials to deliver 10 mA/cm<sup>2</sup>. The first sweep normally suffers from residual and capacitance currents. The sweeps were corrected against the cell potential drop (IR compensation).

As per results shown in (Figure 3.20 to Figure 3.27), sulfurized nickel has shown the lowest overpotential (Figure 3.23). The sample without sulfurized nickel shows the overpotential of 380 mV. When sulfurization of the samples carried out and tested, It shown good amount of decrease in overpotential as it drops down from 380 mV to 311

mV. The results have shown after sulfurization, there is decrease in all sample's overpotential. The reason behind that is sulfur impose mobility interference which lowers its electrical conductivity effect in the host materials, and therefore the improvement of the electrical conductivity of materials by sulfur-donated electrons. The curves for 1 and 1000 cycles were very close, showing the good electrochemical stability of the samples.

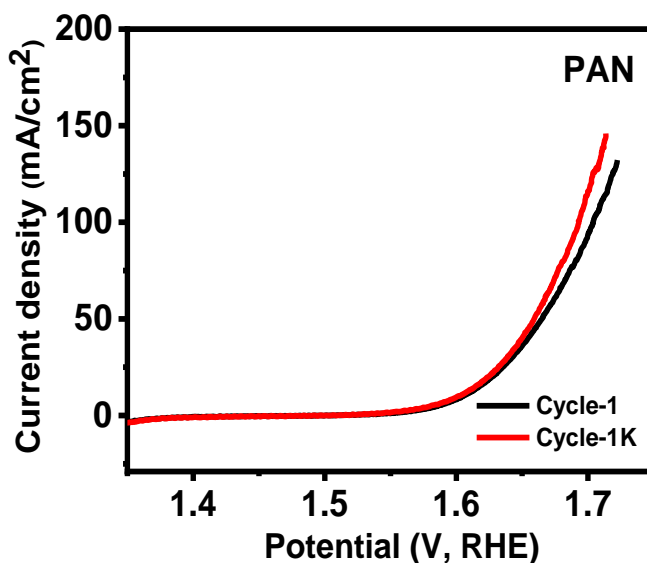


Figure 0.20: LSV curves of PAN at 1 and 1000 cycles

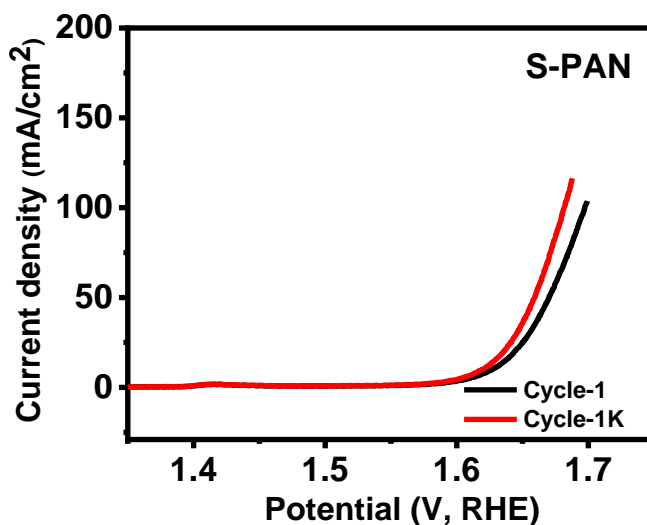


Figure 0.21: LSV curves of S-PAN at 1 and 1000 cycles

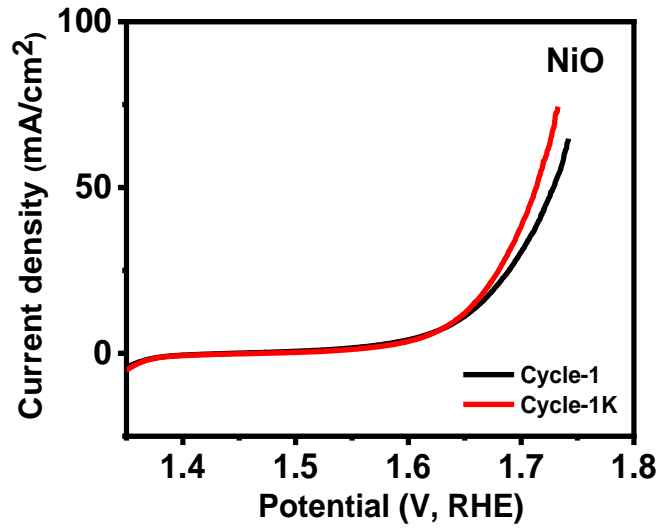


Figure 0.22: LSV curves of NiO at 1 and 1000 cycles

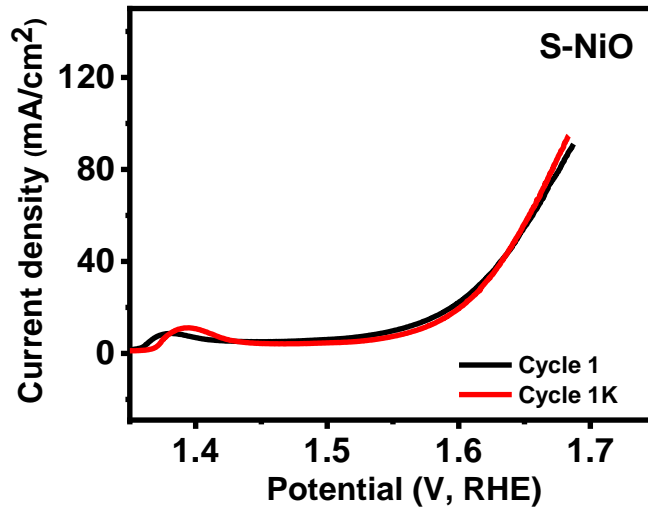


Figure 0.23: LSV curves of S-NiO at 1 and 1000 cycles

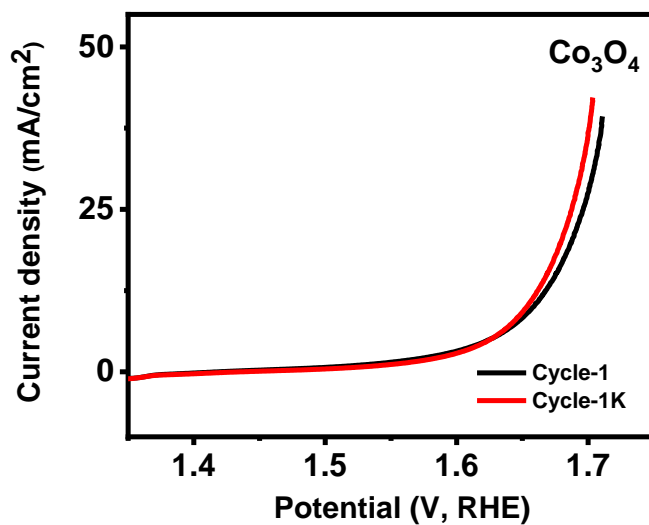


Figure 0.24: LSV curves of  $\text{Co}_3\text{O}_4$  at 1 and 1000 cycles

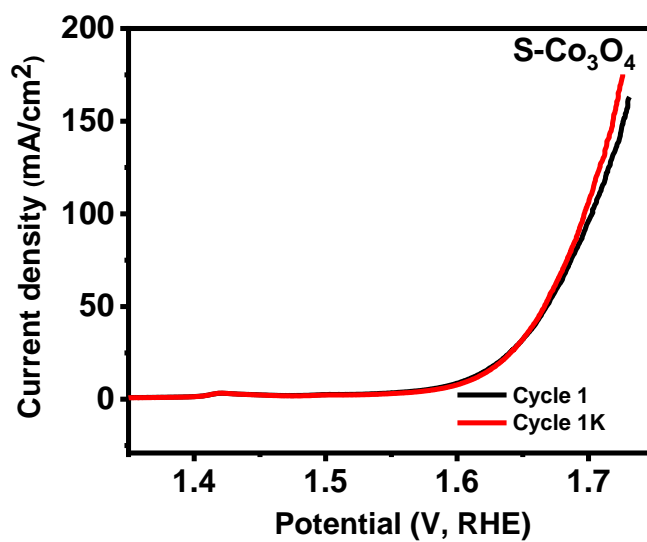


Figure 0.25: LSV curves of  $\text{S-Co}_3\text{O}_4$  at 1 and 1000 cycles

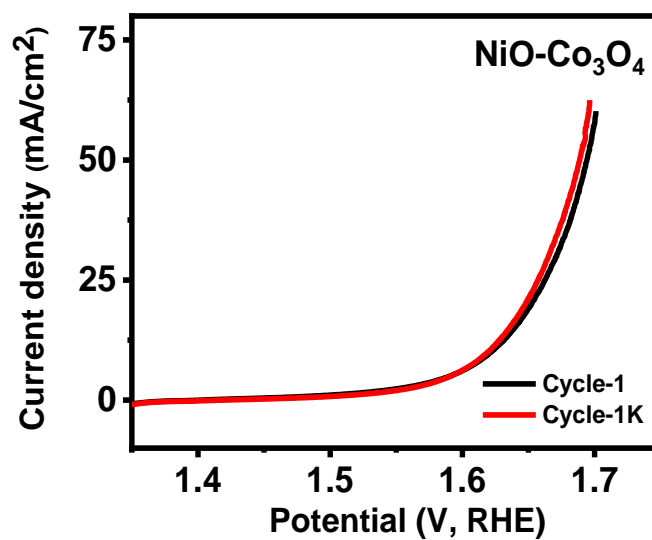


Figure 0.26: LSV curves of NiO-Co<sub>3</sub>O<sub>4</sub> at 1 and 1000 cycles

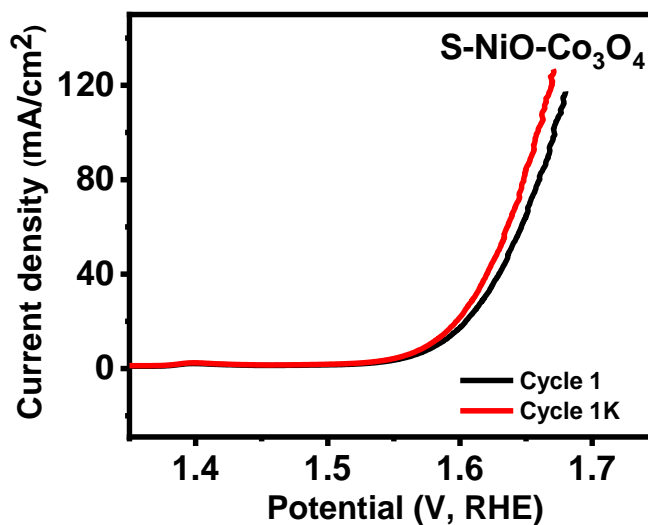


Figure 0.27: LSV curves of S-NiO-Co<sub>3</sub>O<sub>4</sub> at 1 and 1000 cycles

#### 1.9.4 Electrocatalyst for Hydrogen Evolution Reaction

The hydrogen evolution reaction of samples was carried out. The electrocatalytic results were performed at the scanning rate of 2 mV/s in 1M KOH. The HER linear sweep voltammetry polarization curves with their overpotentials are shown in **Figure 3.28** to

**Figure 3.35.** Figure 3.34 shows the combination of NiO and Co<sub>3</sub>O<sub>4</sub>, shows the greatest result for the HER. NiO-Co<sub>3</sub>O<sub>4</sub> shows the minimum overpotential of 96 mV. **Figure 3.35,** 1sulfurized NiO-Co<sub>3</sub>O<sub>4</sub> shows the same overpotential. All other samples synthesized also show good performance PAN (142 mV), S- PAN (149 mV) , NiO (114 mV), S- NiO (121 mV), Co<sub>3</sub>O<sub>4</sub> (128 mV), S- Co<sub>3</sub>O<sub>4</sub> (128 mV). There was no significant change found in the sulfurized samples for HER. The LSV curves of all samples at 1 and 1000 cycles were very close, indicating the material stability.

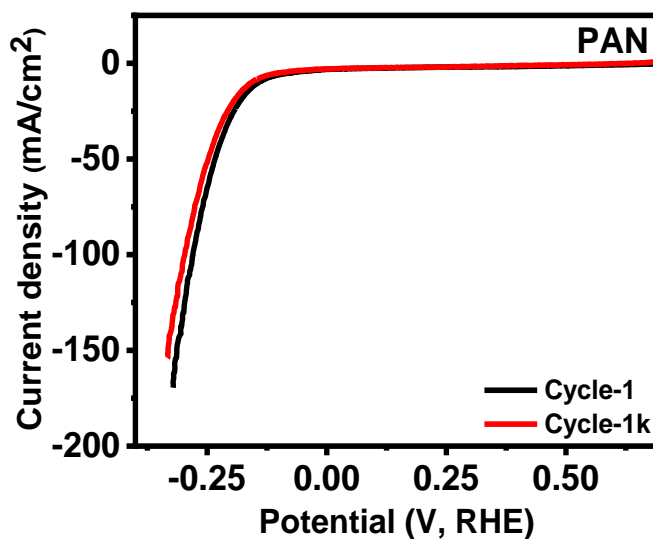


Figure 0.28: LSV curves of PAN at 1 and 1000 cycles

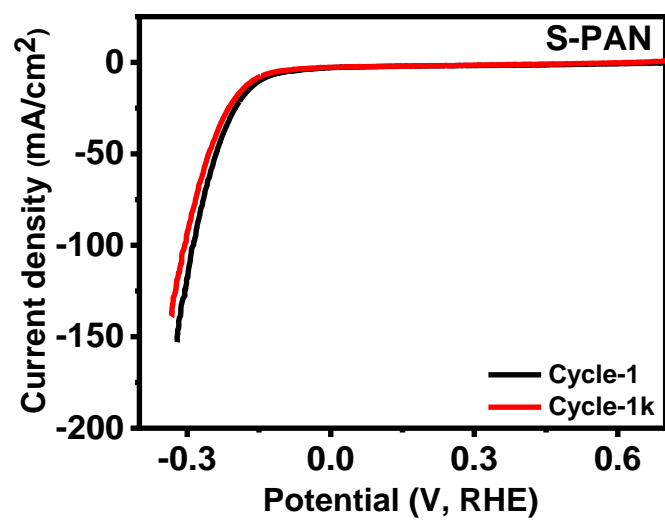


Figure 0.29: LSV curves of S-PAN at 1 and 1000 cycles

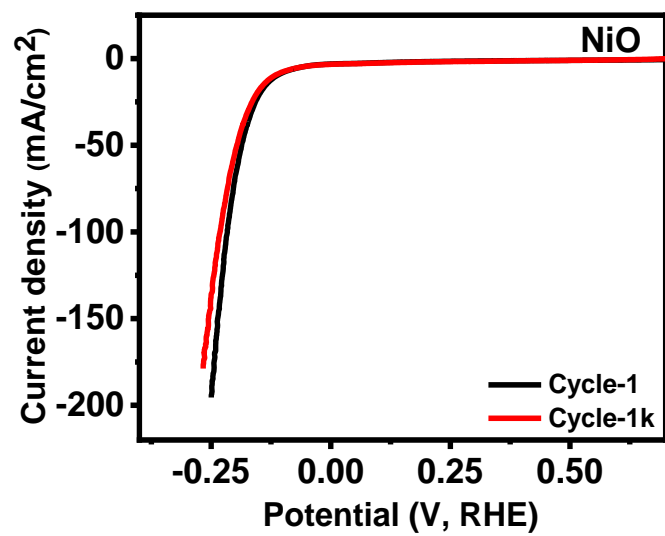


Figure 0.30: LSV curves of NiO at 1 and 1000 cycles

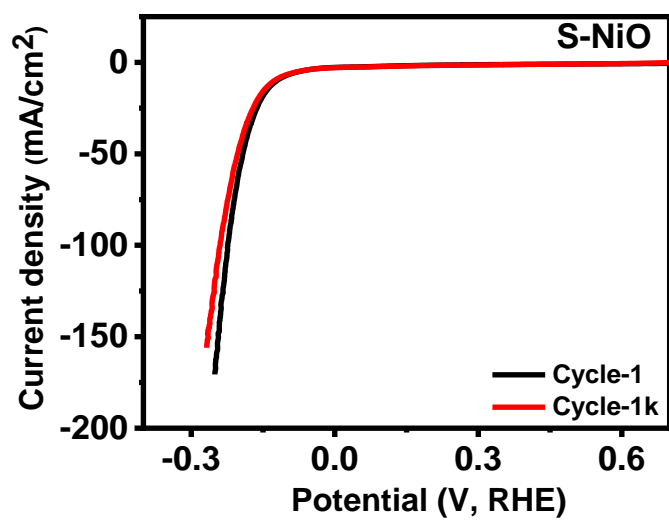


Figure 0.31: LSV curves of S-NiO at 1 and 1000 cycles

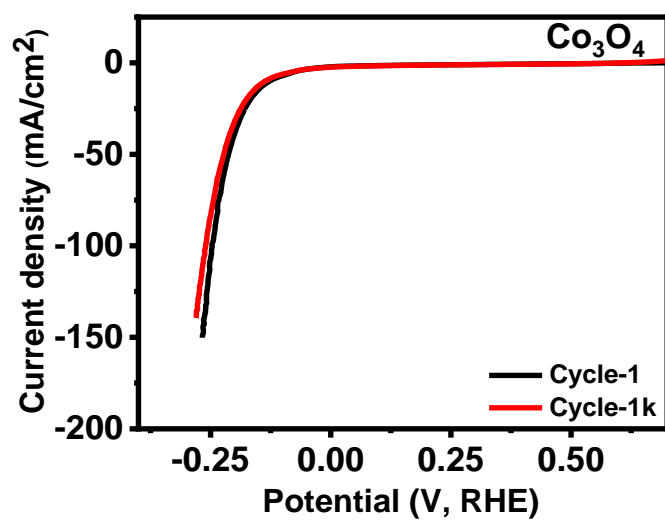


Figure 0.32: LSV curves of Co<sub>3</sub>O<sub>4</sub> at 1 and 1000 cycles

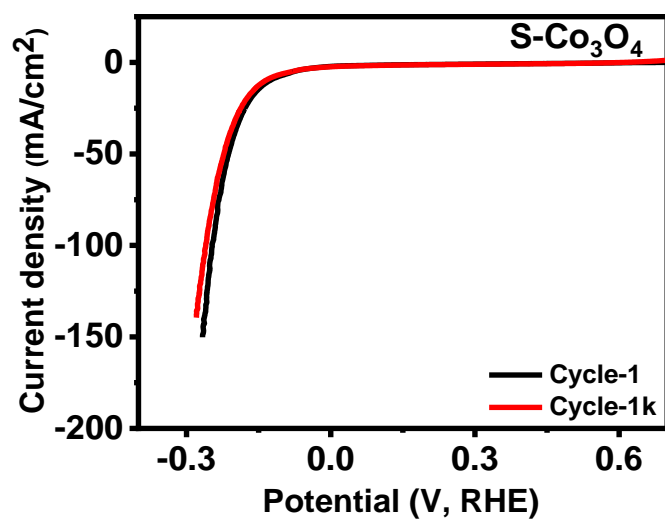


Figure 0.33: LSV curves of S-Co<sub>3</sub>O<sub>4</sub> at 1 and 1000 cycles

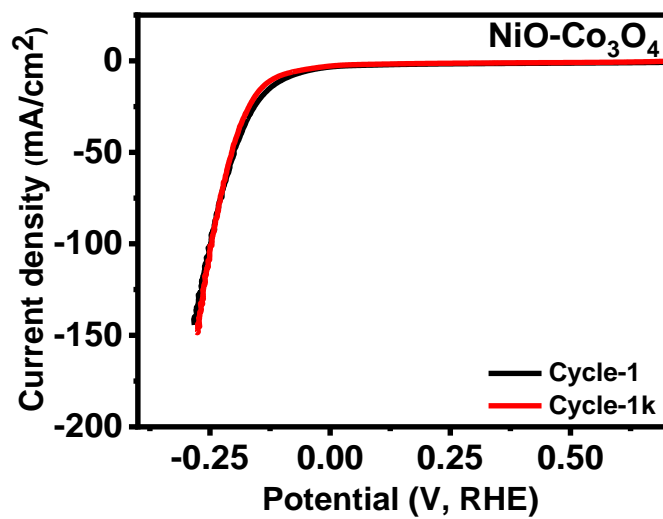


Figure 0.34: LSV curves of NiO-Co<sub>3</sub>O<sub>4</sub> at 1 and 1000 cycles

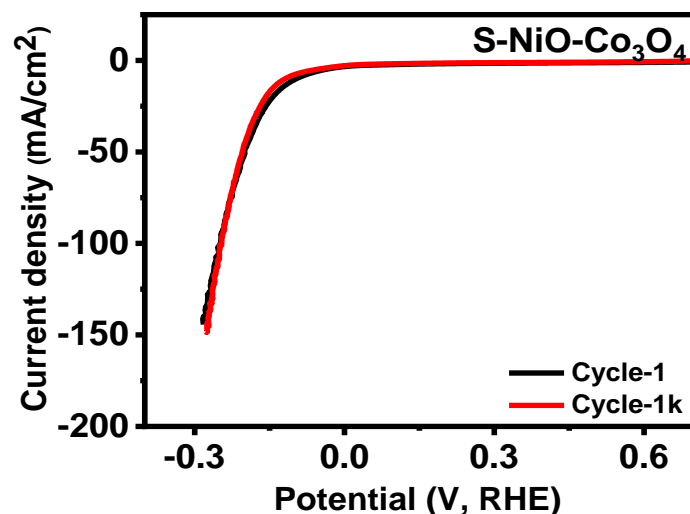


Figure 0.35: LSV curves of S-NiO-Co<sub>3</sub>O<sub>4</sub> at 1 and 1000 cycles

### 1.9.5 Tafel Slope

Tafel analysis is usually employed to understand the reaction kinetics and to compare the catalytic activity of different catalysts. The Tafel slope also helps to define the rate determining step by examining the sensitivity of the current response to the given voltage. The quality of good OER is that it should have a low Tafel slope and large current density. The results of Tafel slope, obtained for OER and HER, in this study are shown by the **Figure 3.36** and **Figure 3.37**. When **Figure 3.36** and **Figure 3.37** were compared, it can be seen that the sulfurized sample in **Figure 3.37** has a lower Tafel slope than the unsulfurized sample.

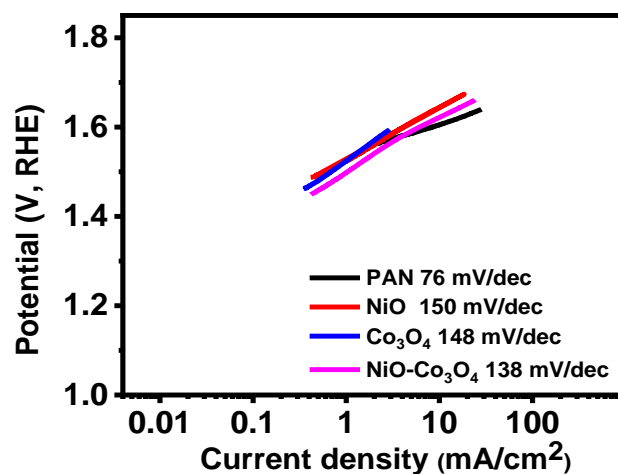


Figure 0.36: OER Tafel plots of PAN, NiO, Co<sub>3</sub>O<sub>4</sub>, and NiO-Co<sub>3</sub>O<sub>4</sub> samples

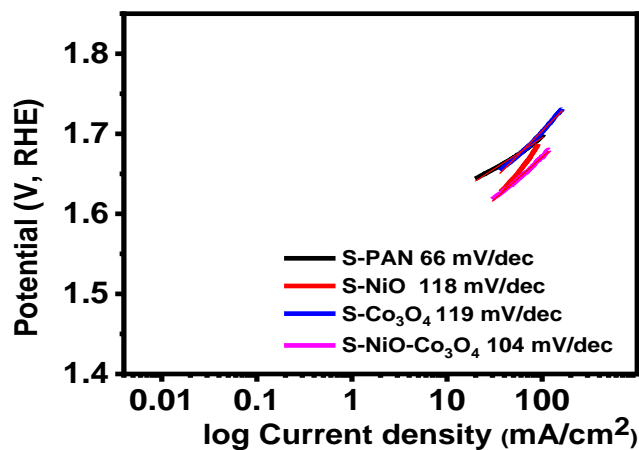


Figure 0.37: OER Tafel plots of S-PAN, S-NiO, S-Co<sub>3</sub>O<sub>4</sub>, and S-NiO-Co<sub>3</sub>O<sub>4</sub> samples.

### 1.9.6 Electrochemical Impedance Spectroscopy

For the assessment of the internal resistance of the prepared materials, electrochemical impedance spectroscopy technique was implemented.

The sulfurized samples seemed to have lower resistance. This is evidenced from the results, When **Figure 3.38**, **Figure 3.40**, **Figure 3.41** and **Figure 3.43** were compared

with their sulfurized version shown in **Figure 3.39**, **Figure 3.41**, **Figure 3.42** and **Figure 3.44**, the impedance of the sulfurized materials was decreased.

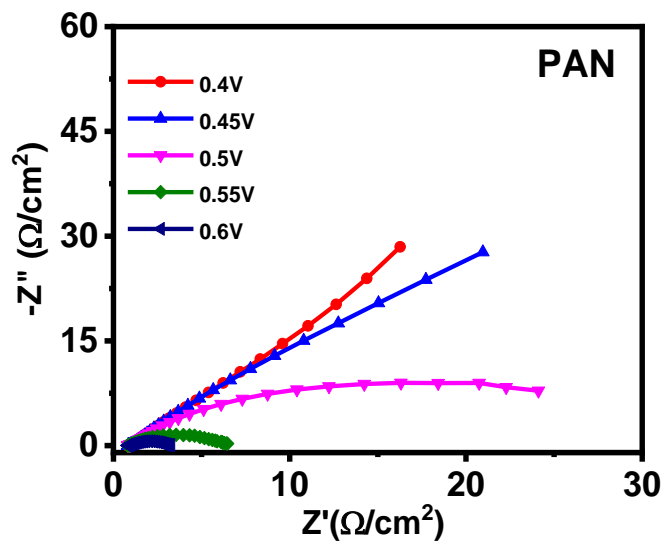


Figure 0.38: Zim versus Zre of PAN at different potentials

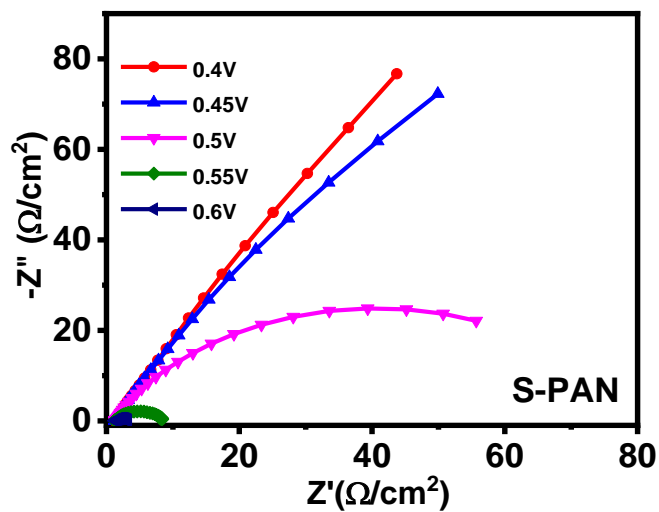


Figure 0.39: Zim versus Zre of S-PAN at different potentials

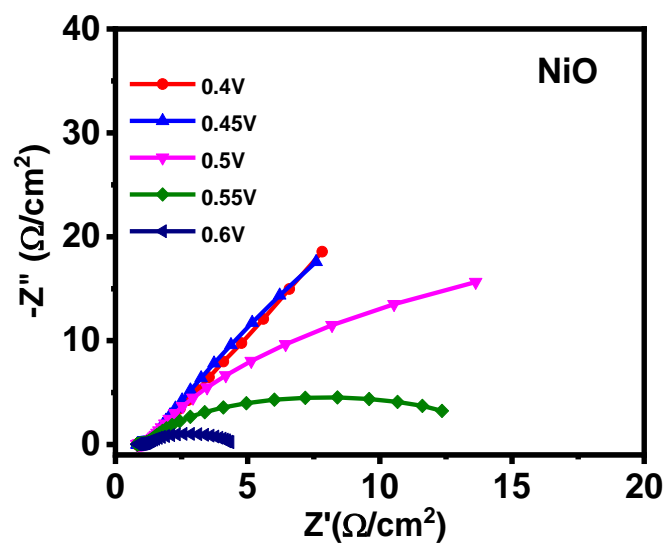


Figure 0.40:  $Z_{im}$  versus  $Z_{re}$  of NiO at different potentials

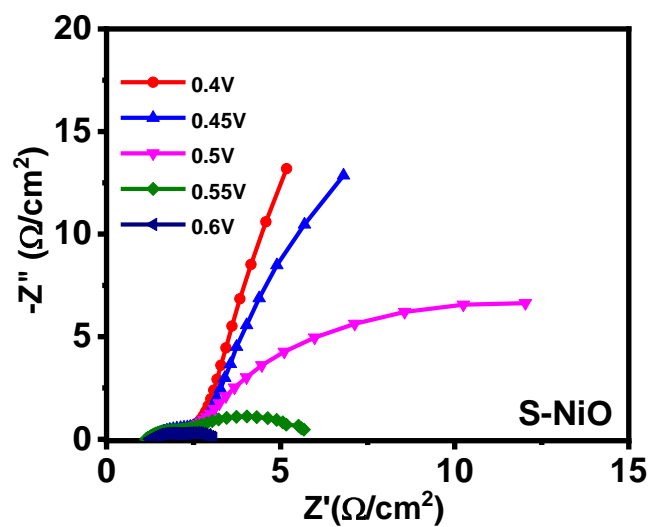


Figure 0.41:  $Z_{im}$  versus  $Z_{re}$  of S- NiO at different potentials

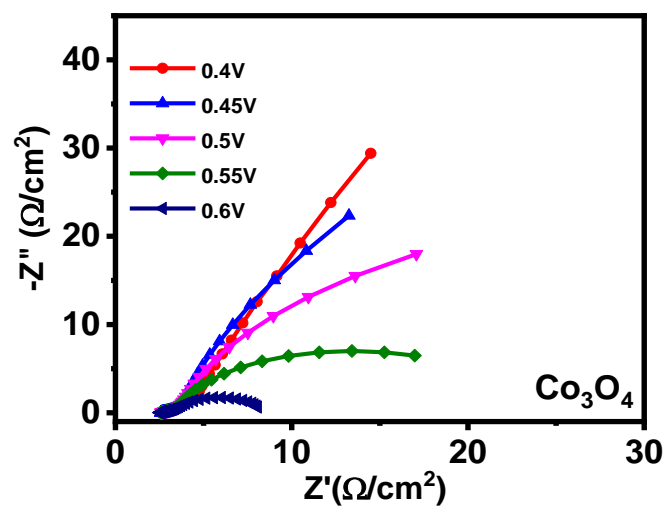


Figure 0.42: Zim versus Zre of  $\text{Co}_3\text{O}_4$  at different potentials

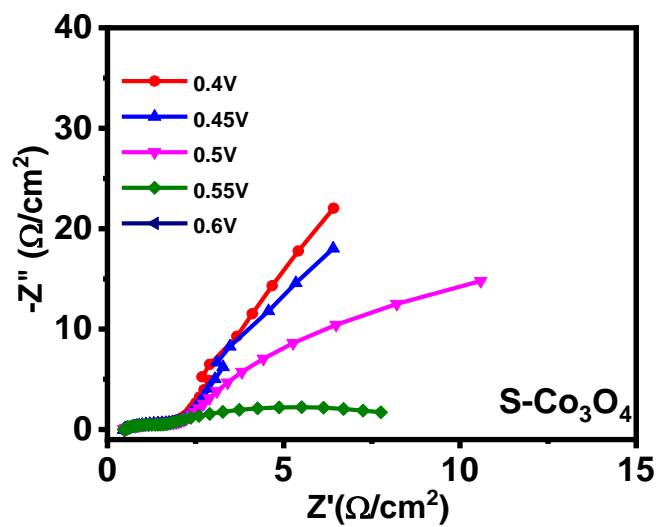


Figure 0.43: Zim versus Zre of  $\text{S-Co}_3\text{O}_4$  at different potentials

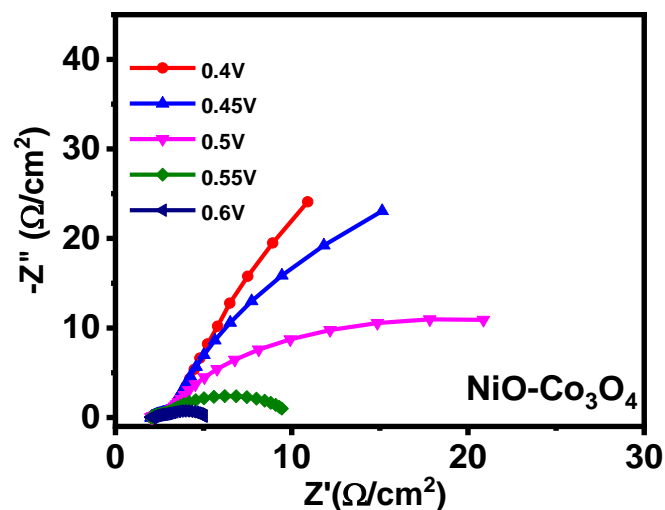


Figure 0.44: Zim versus Zre of NiO-Co<sub>3</sub>O<sub>4</sub> at different potentials

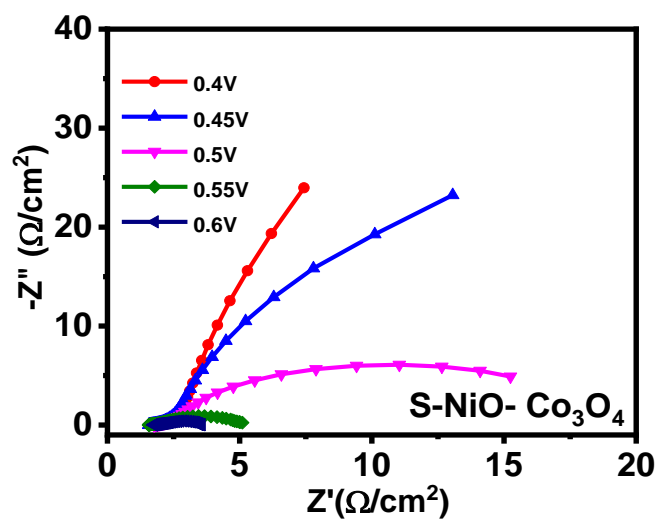


Figure 0.45: Zim versus Zre of S-NiO-Co<sub>3</sub>O<sub>4</sub> at different potentials

### 1.9.7 Scanning Electron Microscope

A scanning electron microscope (SEM) is a type of electron microscope which generates sample images through the process of scanning the surface of materials through the assistance of highly focused electron-based beams. The electrons in the beam interact

with the atoms. As a result of this interaction, electrons produce different types of signals which carry extremely useful information related to the surface topography as well as the composition of the sample. The beam of electrons is first scanned in a raster scan pattern, and later the beam position is attached with the intensity of the detected signal for the production of an image. In most of the commonly used modes of SEM, a secondary electron detector is used to detect the secondary electrons emitted by atoms which are brought in the excited state by the help of passing an electron beam through the material (Everhart-Thornley detector). The number of secondary electrons that can be detected, and thus the signal intensity, depends, among other things, on specimen topography.

The morphological characteristics and structure of the material under study were evaluated using this technique. **Figure 3.46** to **Figure 3.61** represent the images collected through scanning electron microscopy using different magnification levels.

**Figure 3.46** and **Figure 3.47** show the morphology of PAN at different resolutions, the image is clearly showing clustered fiber structure. **Figure 3.54** and **Figure 3.55** show the morphology of the cobalt oxide incorporated PAN fibers, clearly showing the difference in image that cobalt oxide has changed the morphology of the PAN fibers. **Figure 3.50** and **Figure 3.51** show the morphology of the nickel oxide incorporate PAN fibers; it has changed morphology immensely, showing the porous surface on the fibers, which increased the surface area of the fibers. **Figure 3.58** and **Figure 3.59** show the incorporation of the nickel oxide and cobalt oxide mixture in PAN fibers. It does show noticeable porous surface on fibers. **Figure 3.48**, **Figure 3.52**, **Figure 3.56**, and **Figure 3.60** show the sulfurized PAN, NiO,  $\text{Co}_3\text{O}_4$  and NiO- $\text{Co}_3\text{O}_4$  samples respectively. The results shows more irregularity in the size of the fibers because of the sulfurization.

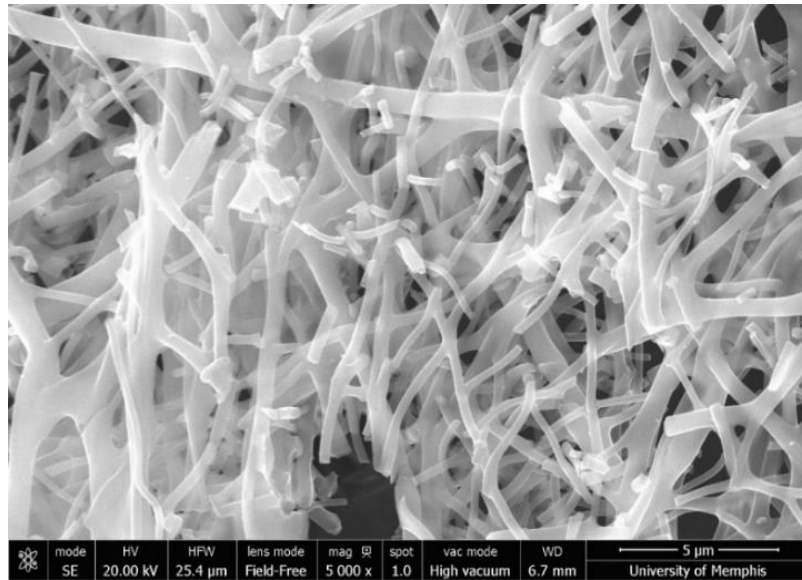


Figure 3.46: SEM image of PAN

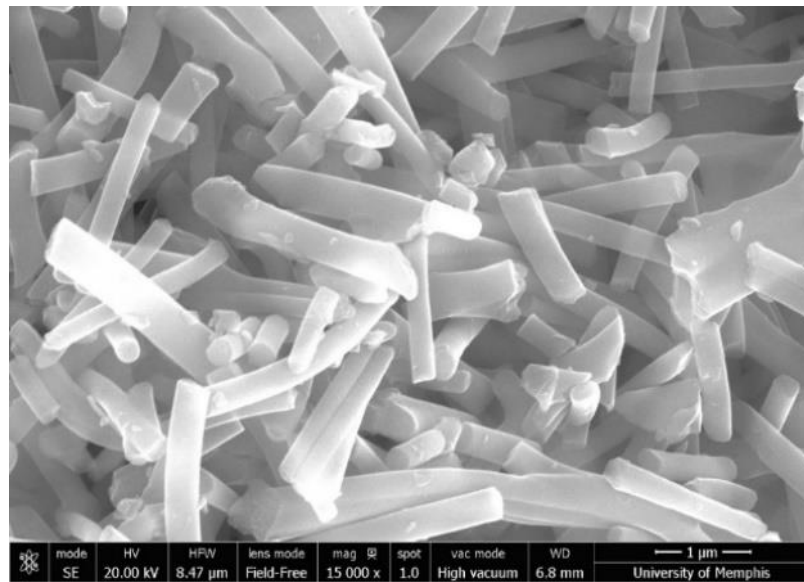


Figure 3.47: SEM image of PAN

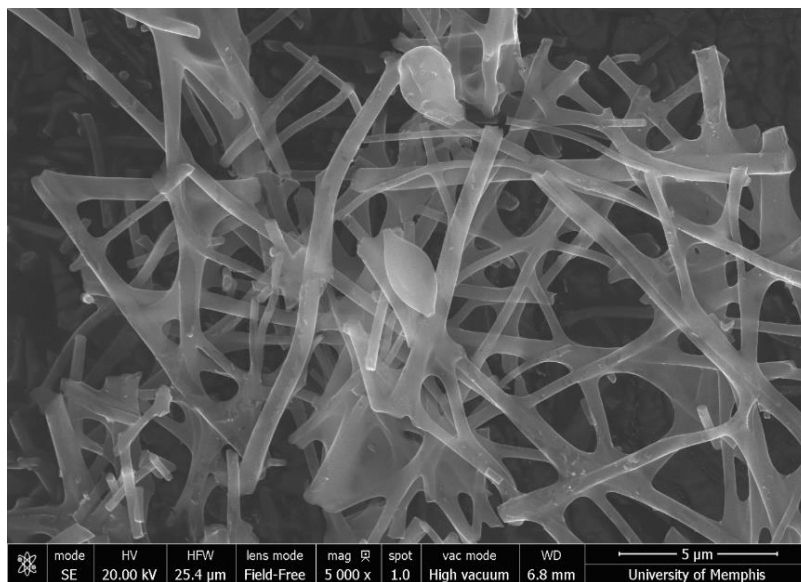


Figure 3.48: SEM image of S-PAN

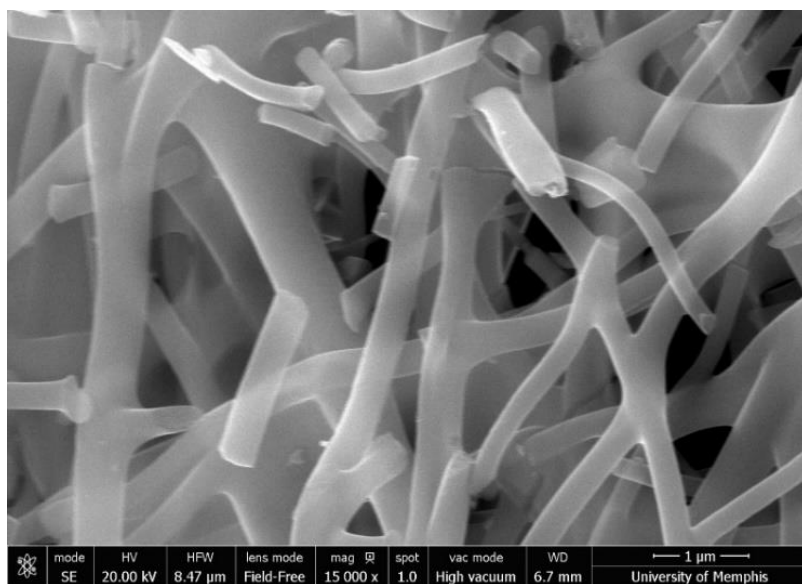


Figure 3.49: SEM image of S-PAN

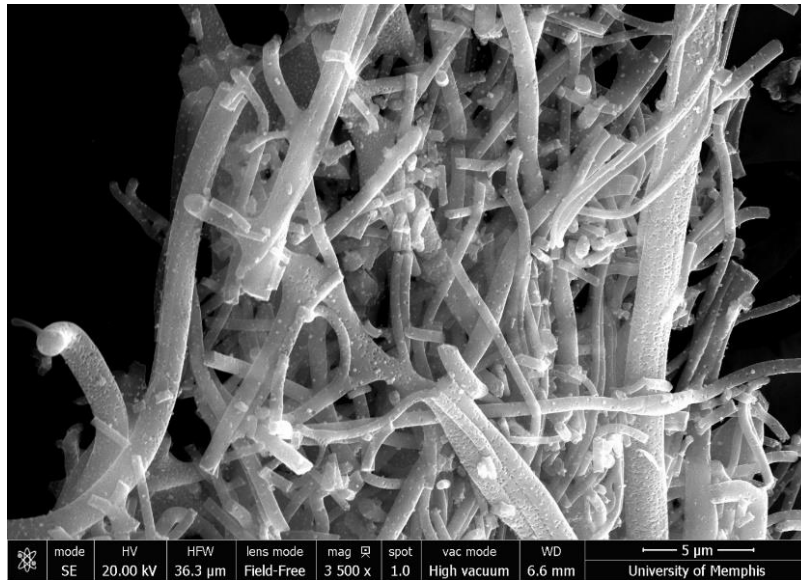


Figure 3.50: SEM image of NiO

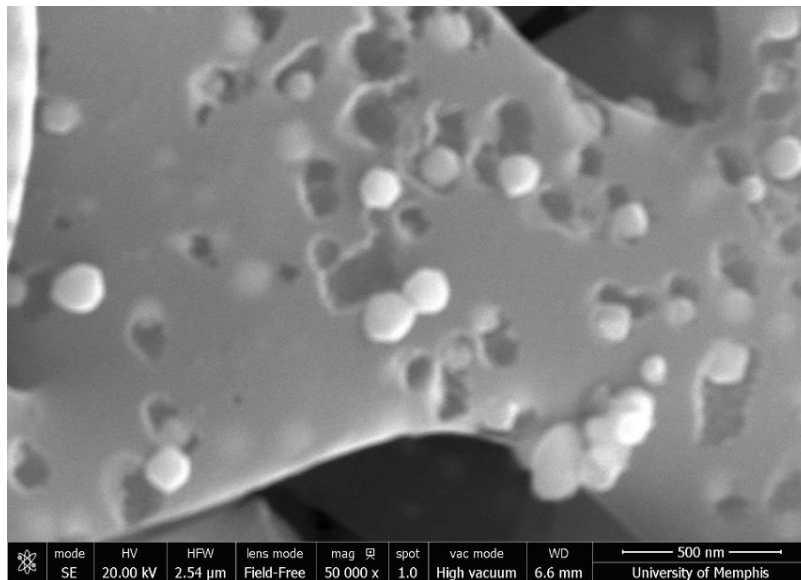


Figure 3.51: SEM image of NiO

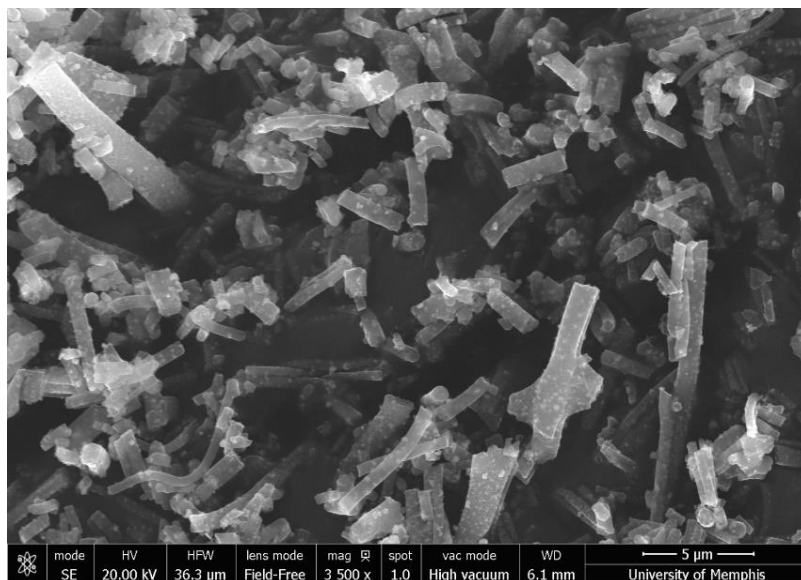


Figure 3.52: SEM image of S-NiO

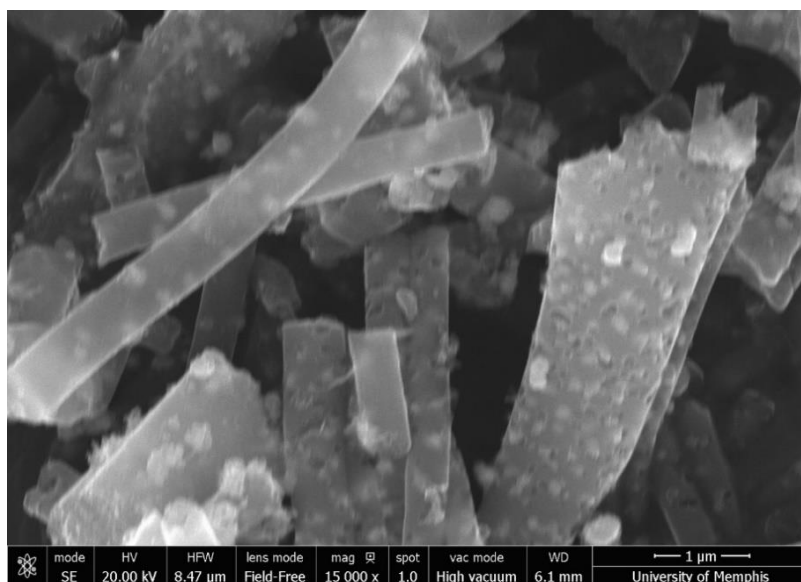


Figure 5.53: SEM image of S-NiO

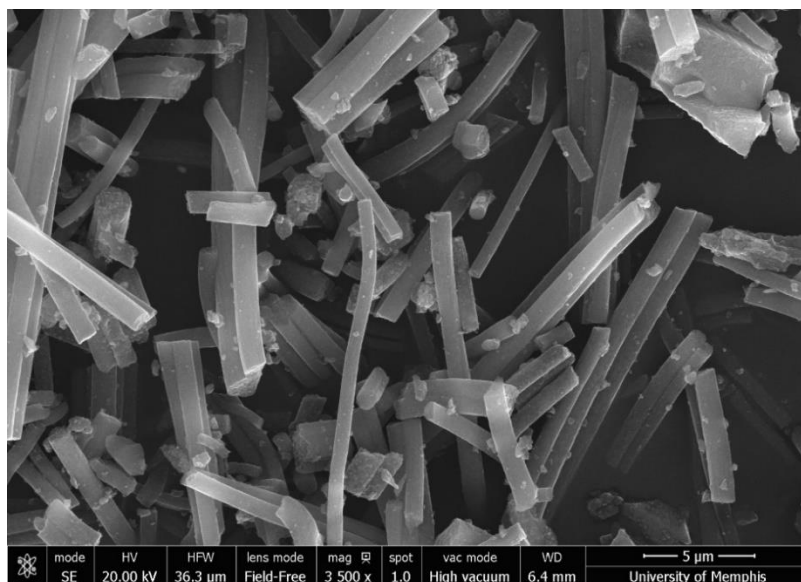


Figure 3.54: SEM image of  $\text{Co}_3\text{O}_4$

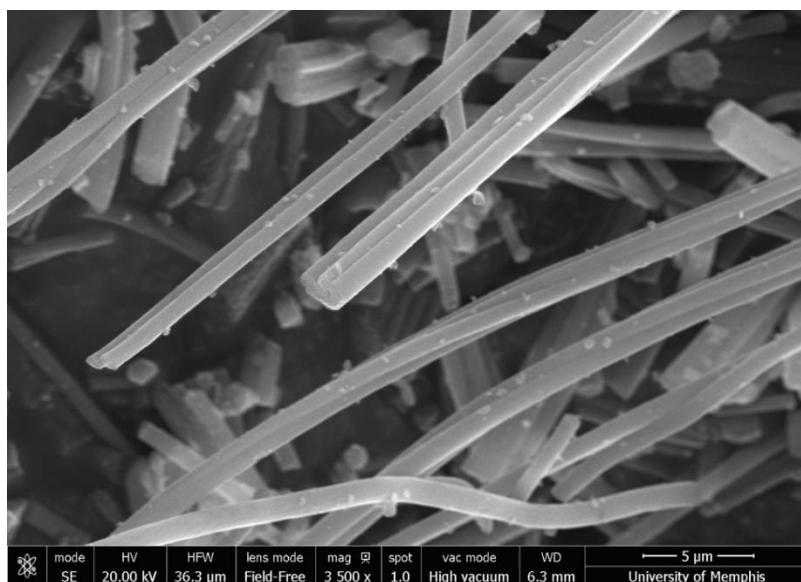


Figure 3.55: SEM image of  $\text{Co}_3\text{O}_4$

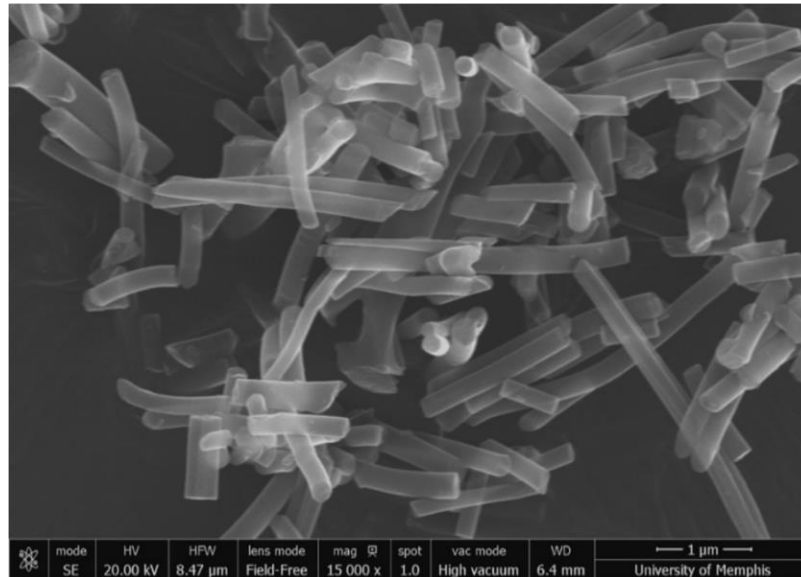


Figure 3.56: SEM image of S-Co<sub>3</sub>O<sub>4</sub>

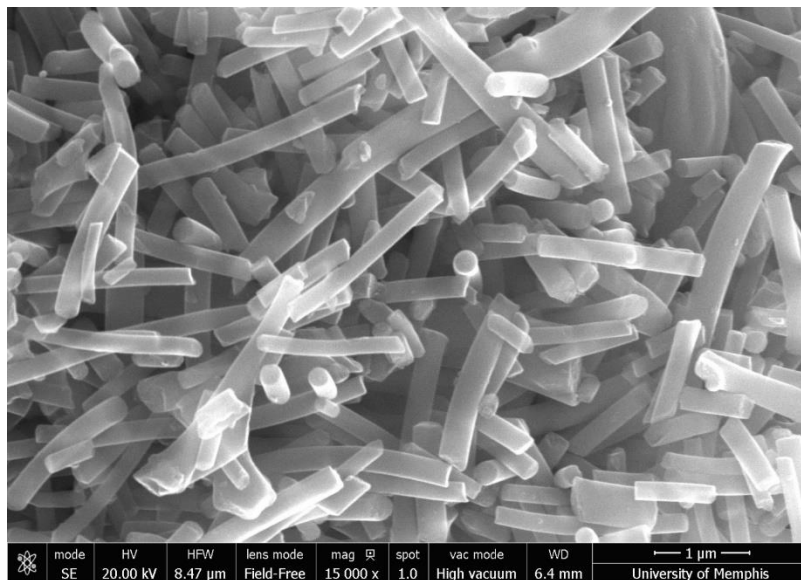


Figure 3.57: SEM image of S-Co<sub>3</sub>O<sub>4</sub>

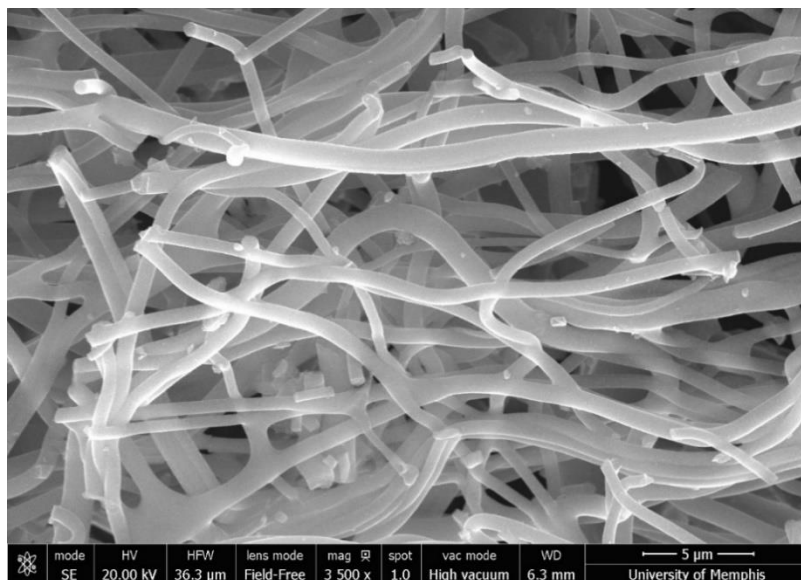


Figure 3.58: SEM image of NiO-Co<sub>3</sub>O<sub>4</sub>

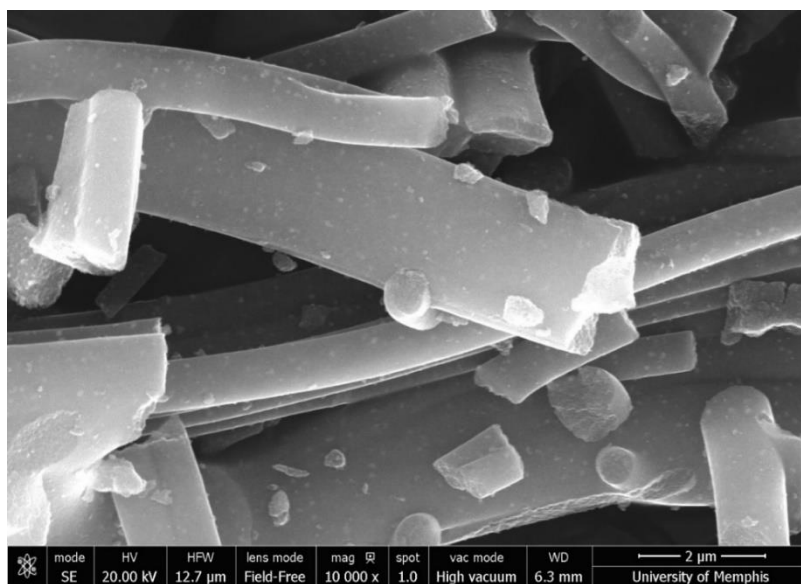


Figure 3.59: SEM image of NiO-Co<sub>3</sub>O<sub>4</sub>

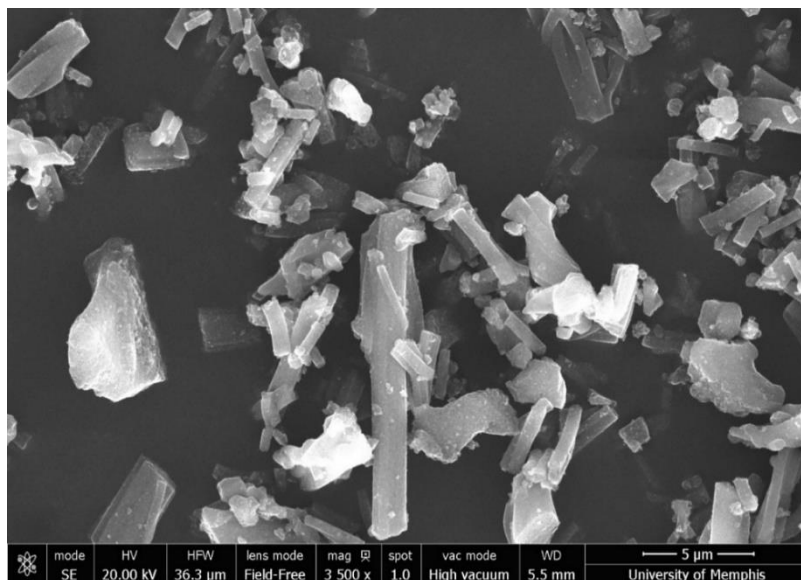


Figure 3.60: SEM image of S-NiO-Co<sub>3</sub>O<sub>4</sub>

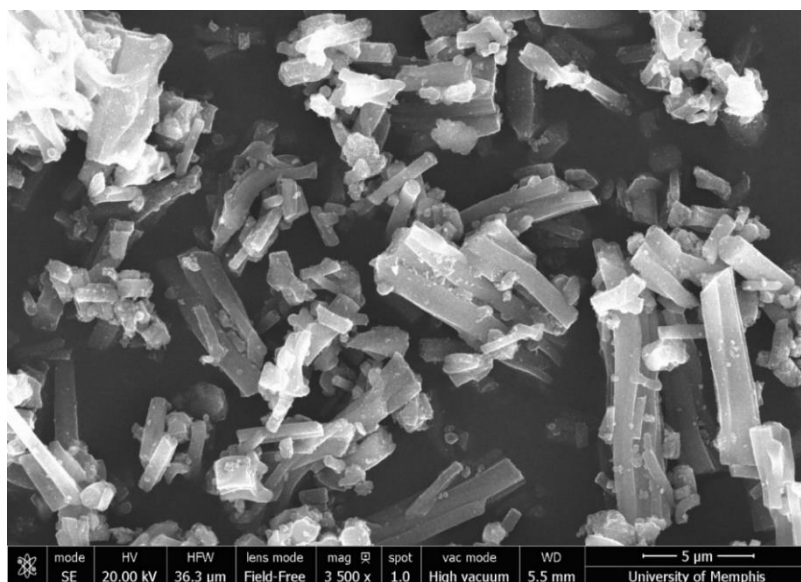


Figure 3.61: SEM image of S-NiO-Co<sub>3</sub>O<sub>4</sub>

### 1.9.8 Electro chemical Stability Test

For the determination of quality as well as durability of the prepared nanomaterials, a stability test was carried out. The results show that the materials were very stable and

capable of permitting a steady flow of current through it. The **Figure 3.62** to **Figure 3.69**, for these tests are given in detail below

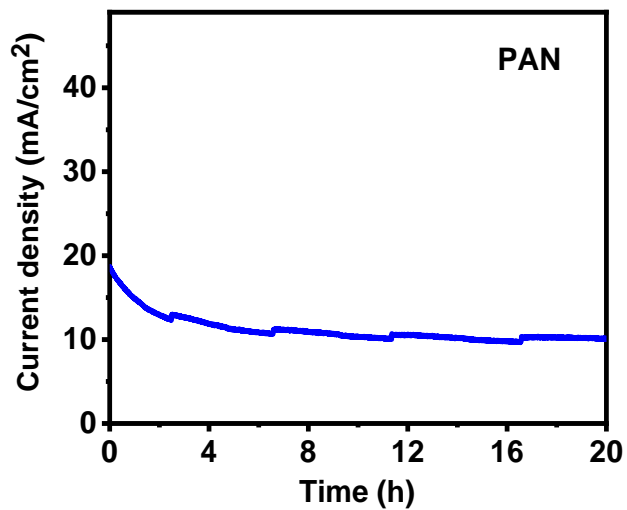


Figure 0.62: CA plot of PAN for 16 hours

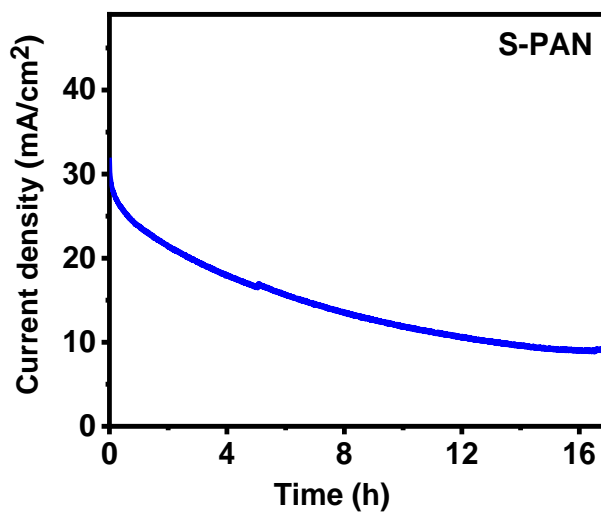


Figure 0.63: CA plot of S-PAN for 16 hours

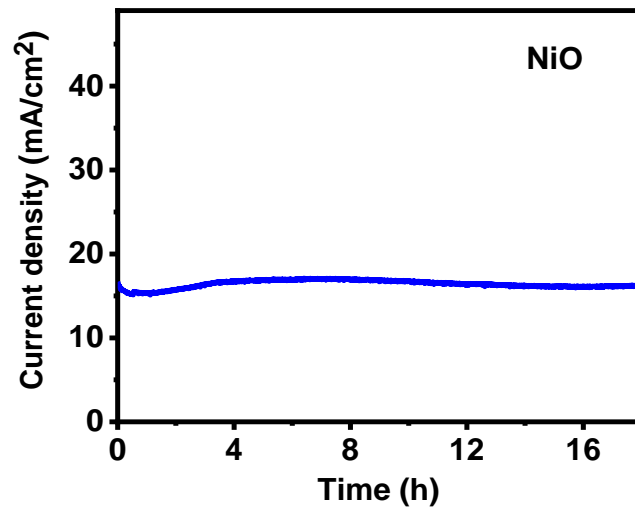


Figure 0.64: CA plot of NiO for 16 hours

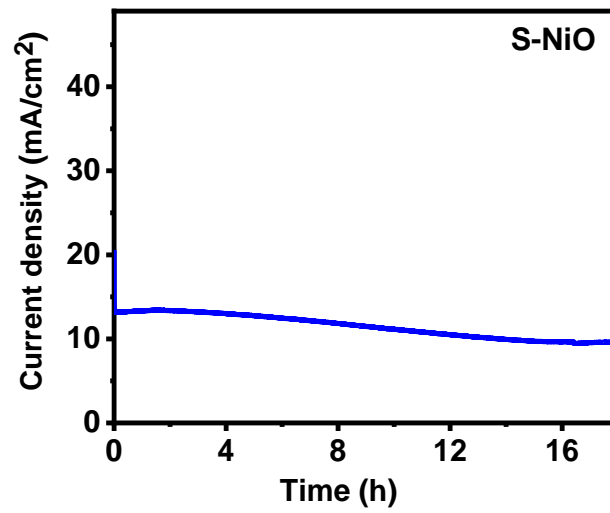


Figure 0.65: CA plot of S-NiO for 16 hours

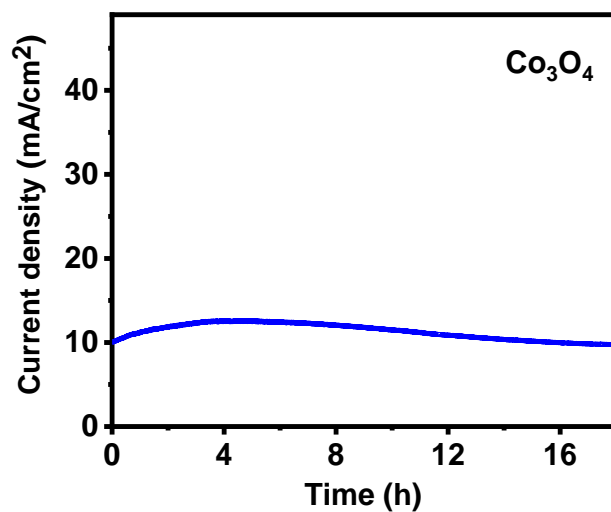


Figure 0.66: CA plot of Co<sub>3</sub>O<sub>4</sub> for 16 hours

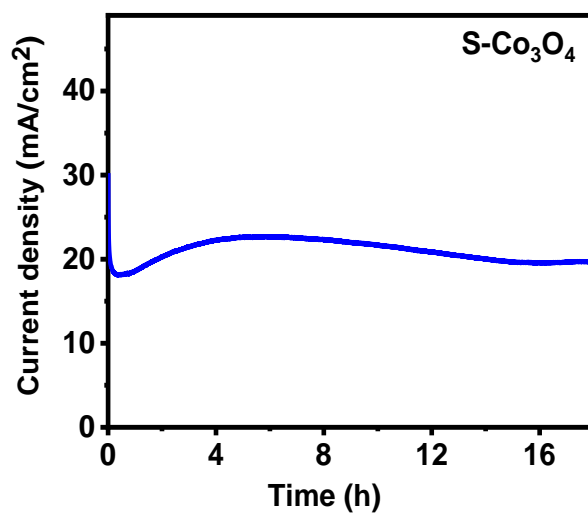


Figure 0.67: CA plot of S-Co<sub>3</sub>O<sub>4</sub> for 16 hours

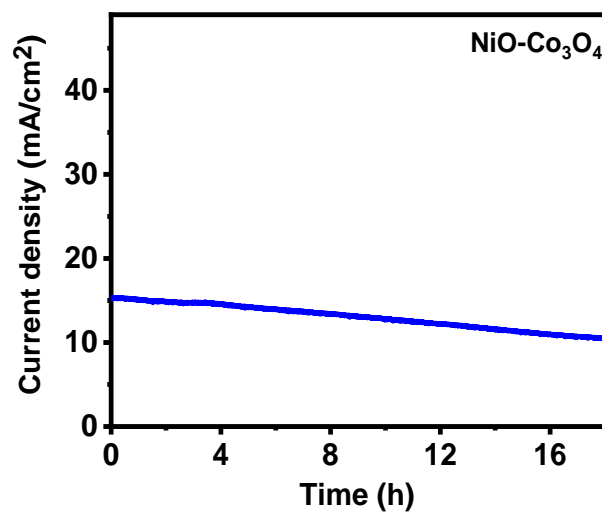


Figure 0.68: CA plot of NiO-Co<sub>3</sub>O<sub>4</sub> for 16 hours

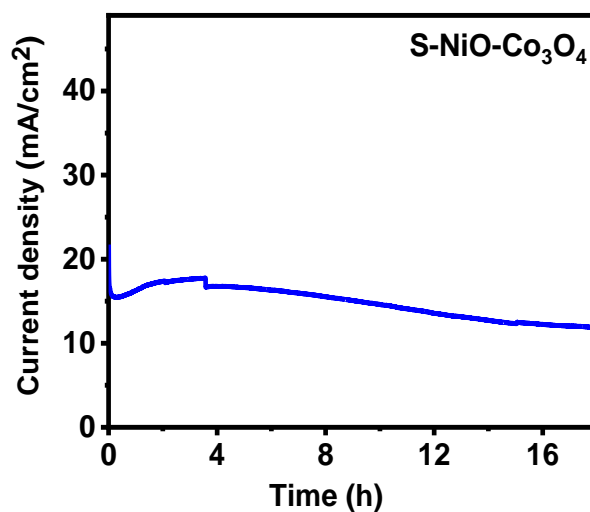


Figure 0.69: CA plot of S-NiO-Co<sub>3</sub>O<sub>4</sub> for 16 hours

### 1.9.9 Electrochemical Stability Test for Supercapacitor

The supercapacitance of the prepared nanomaterials was identified for normal as well as sulfurized samples. The results obtained after carrying out the test are shown in the **Figure 3.70** to **Figure 3.77**. **Figure 3.70** shows the number of cycles versus capacity

retention graph of PAN, where it is losing almost fifty percent of capacitance retention after 5000 cycles. **Figure 3.71** shows the graph for S-PAN, where it is showing the improvement in results, sulfurized PAN sample showed the capacitance retention of ninety five percent after 5000 cycles. **Figure 3.72** and **Figure 3.73** shows the same, sulfurization improved the capacitance retention for NiO sample too. As shown in **Figure 3.74** and **Figure 3.75** cobalt oxides showed good capacitance retention with and without sulfurization. **Figure 3.76** and **Figure 3.77** show the capacitance retention of the mixture of cobalt oxide and nickel oxides sample. They also show consistent capacitance retention after 5000 cycles for sulfurized and unsulfurized samples.

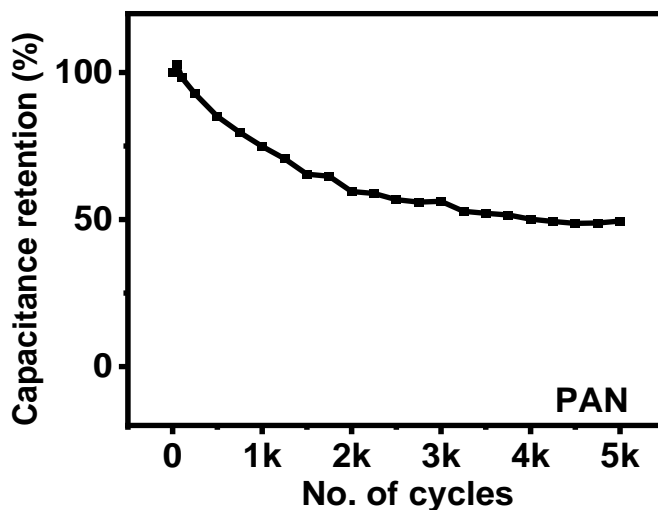


Figure 0.70: Number of cycles versus capacitance retention of PAN

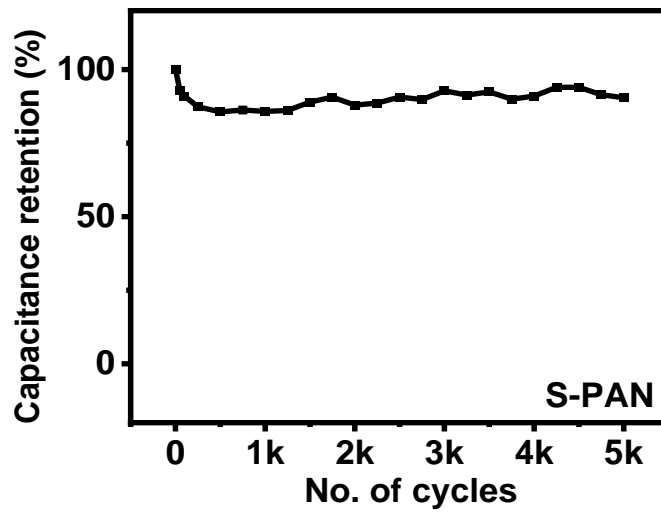


Figure 0.71: Number of cycles versus capacitance retention S-PAN

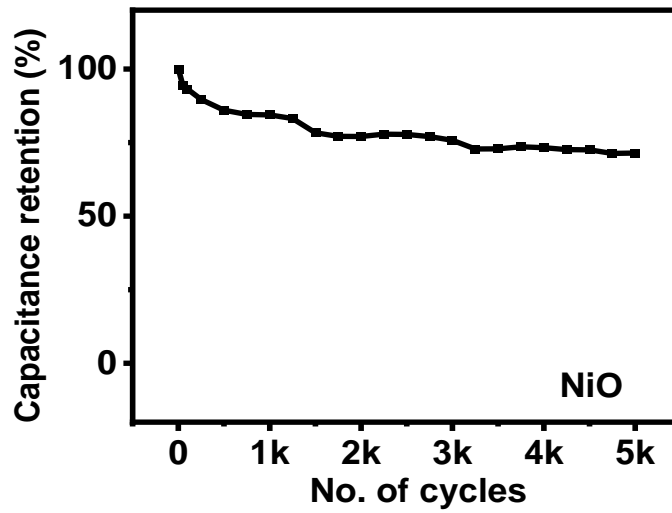


Figure 0.72: Number of cycles versus capacitance retention of NiO

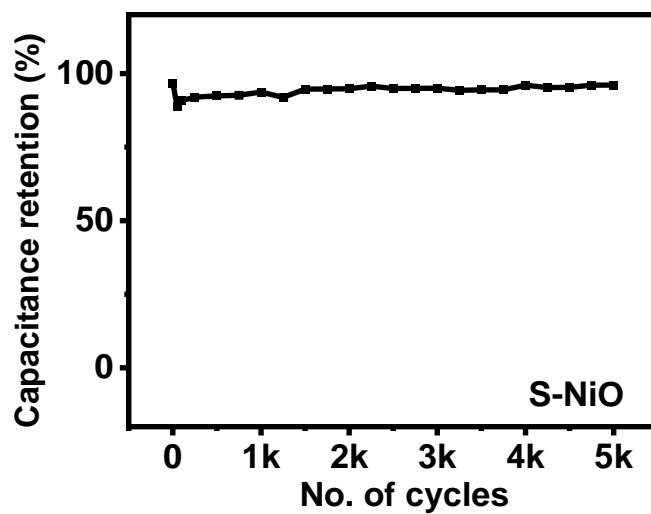


Figure 0.73: Number of cycles versus capacitance retention of S-NiO

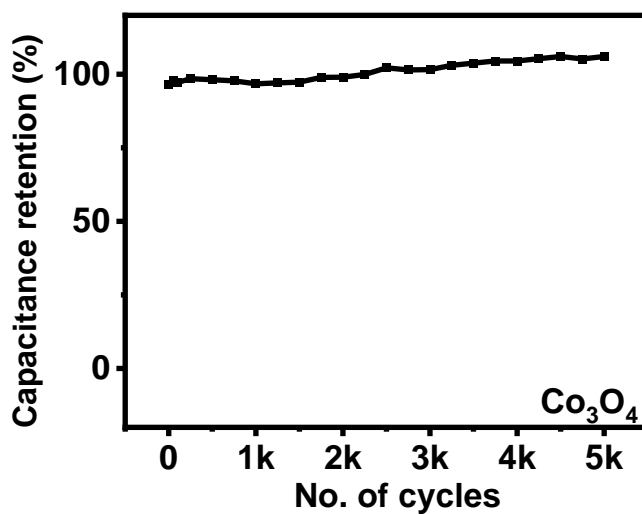


Figure 0.74: Number of cycles versus capacitance retention of Co<sub>3</sub>O<sub>4</sub>

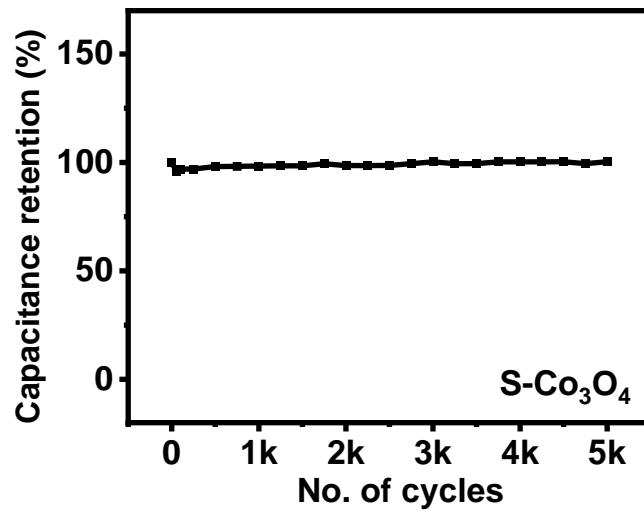


Figure 0.75: Number of cycles versus capacitance retention of S-Co<sub>3</sub>O<sub>4</sub>

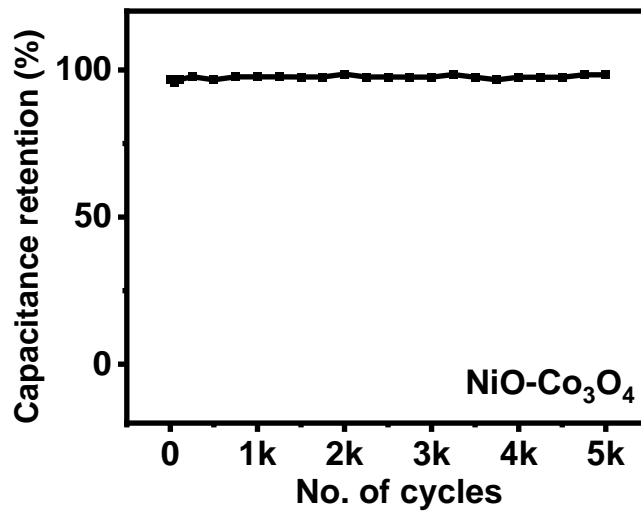


Figure 3.76: Number of cycles versus capacitance retention of NiO-Co<sub>3</sub>O<sub>4</sub>

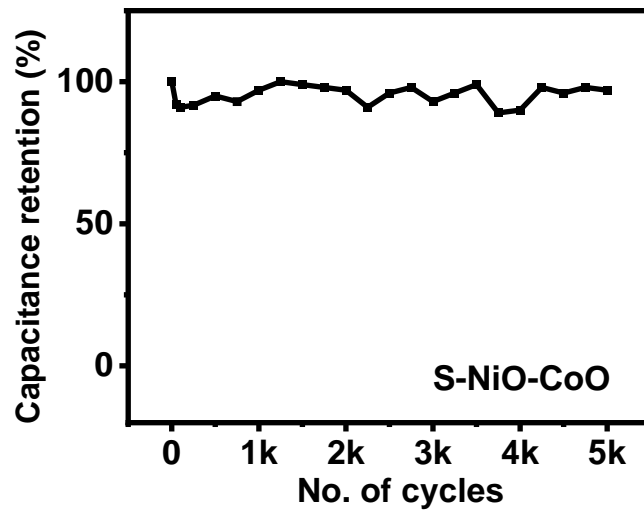


Figure 0.77: Number of cycles versus capacitance retention S-NiO-Co<sub>3</sub>O<sub>4</sub>

## CHAPTER IV

### CONCLUSION

#### 1.10 Conclusions

The results revealed that the synthesized materials and fibers can prove themselves to be a promising alternate for the storage of energy. The materials used for the evaluation under this study include N, N-dimethylformamide (DMF), Ni (NO<sub>3</sub>)<sub>2</sub> · 6H<sub>2</sub>O, polyacrylonitrile, Co (NO<sub>3</sub>)<sub>2</sub> · 6H<sub>2</sub>O. The required fibers were developed in a total of three stages. During the first stage, a homogenous mixture was prepared. During the second stage, the solution was subject to electrospinning. In the third stage, the prepared nanofibers were calcinated to produce the 1D nanofibers of metal oxides.

The samples were tested for supercapacitor applications, hydrogen evolution reaction and oxygen evolution reactions. There was a set back with the results obtained for supercapacitor application. Results for oxygen evolution reaction were valuable. The samples which contained the NiO showed overpotential of the 380 mV. The results that were obtained from hydrogen evolution reaction were impressive as well. The sample containing the combination of both NiO and Co<sub>3</sub>O<sub>4</sub> proved to be the best amongst all. The combination of NiO and Co<sub>3</sub>O<sub>4</sub> showed overpotential of 96 mV.

Furthermore, all other samples were studied using the sulfurized process. The results for OER performance, sulfurized NiO were easily distinguished; it changed from 380 mV

overpotential to 311 mV. While remarkable, sulfurization did not change any performance for the hydrogen evolution reactions. For supercapacitor application, the sulfurized nickel oxide sample showed that it increased capacitance from 94 F/g to 215 F/g,

Lastly, to sum up, the materials fabricated for these experiments show good results for the HER and OER application. Usually, the overpotential that lies between 300 mV and 400 mV for the OER application is considered good material [53]. The material (S-NiO) that has been fabricated in this study shows the overpotential of 311 mV, which is counted as an acceptable and a desirable outcome. Alternatively, for HER application the best material available so far is platinum which shows the overpotential of 70 mV. The study for HER applications demonstrates that any material used that results in overpotential under 100 mV is considered good material [54]. The material (S- NiO-Co<sub>3</sub>O<sub>4</sub>) that has been fabricated for this study showed overpotential of 96 mV, which is considered the use of good material for the HER performance.

## REFERENCES

- [1]. Asif, M., & Muneer, T. (2007). Energy supply, its demand and security issues for developed and emerging economies. *Renewable and sustainable energy reviews*, 11(7), 1388-1413.
- [2]. Santoro, C., Arbizzani, C., Erable, B., & Ieropoulos, I. (2017). Microbial fuel cells: From fundamentals to applications. A review. *Journal of power sources*, 356, 225-244.
- [3]. Kouchachvili, L., Yaïci, W., & Entchev, E. (2018). Hybrid battery/supercapacitor energy storage system for the electric vehicles. *Journal of Power Sources*, 374, 237-248.
- [4]. Jalonsom (2016). Wind Turbine Schematic. Available at [https://commons.wikimedia.org/wiki/File:Wind\\_turbine\\_schematic.svg](https://commons.wikimedia.org/wiki/File:Wind_turbine_schematic.svg).
- [5]. Energy explained. (2021). Hydropower explained. US Energy Information Administration. Available at <https://www.eia.gov/energyexplained/hydropower/>.
- [6]. Amrit Kumar. Geothermal Energy-Definition, Working Diagram/Layout, Examples, PDF, available at <https://learnmechanical.com/geothermal-energy/>.
- [7]. Sharma, S., Jain, K. K., & Sharma, A. (2015). Solar cells: in research and applications—a review. *Materials Sciences and Applications*, 6(12), 1145.

- [8]. Winter, M., & Brodd, R. J. (2004). What are batteries, fuel cells, and supercapacitors?. *Chemical reviews*, 104(10), 4245-4270.
- [9]. Digital buyers guide (2016). Lithium Primary Batteries, available at <https://korean-electronics.com/tag/lithium-primary-batteries/>.
- [10]. Mohit R., Secondary Batteries (Lead-Acid Battery), available at [https://edurev.in/studytube/Secondary-Batteries--Lead-Acid-Battery-/9a00a318-14d0-4d1a-adbd-d4d779d394d4\\_t](https://edurev.in/studytube/Secondary-Batteries--Lead-Acid-Battery-/9a00a318-14d0-4d1a-adbd-d4d779d394d4_t)
- [11]. Murray-Smith, David. (2019). A Review of Developments in Electrical Battery, Fuel Cell and Energy Recovery Systems for Railway Applications A Report for the Scottish Association for Public Transport. 10.13140/RG.2.2.16555.67362.
- [12]. Lin, Z., Goikolea, E., Balducci, A., Naoi, K., Taberna, P. L., Salanne, M., ... & Simon, P. (2018). Materials for supercapacitors: When Li-ion battery power is not enough. *Materials today*, 21(4), 419-436.
- [13]. Hao, Z. Q., Cao, J. P., Wu, Y., Zhao, X. Y., Zhuang, Q. Q., Wang, X. Y., & Wei, X. Y. (2017). Preparation of porous carbon sphere from waste sugar solution for electric double-layer capacitor. *Journal of Power Sources*, 361, 249-258.
- [14]. Raj, C. J., Rajesh, M., Manikandan, R., Yu, K. H., Anusha, J. R., Ahn, J. H., ... & Kim, B. C. (2018). High electrochemical capacitor performance of oxygen and nitrogen enriched activated carbon derived from the pyrolysis and activation of squid gladius chitin. *Journal of Power Sources*, 386, 66-76.

- [15]. Zhou, L., Li, C., Liu, X., Zhu, Y., Wu, Y., & van Ree, T. (2018). Metal oxides in supercapacitors. In *Metal Oxides in Energy Technologies* (pp. 169-203). Elsevier.
- [16]. Lu, Q., Chen, J. G., & Xiao, J. Q. (2013). Nanostructured electrodes for high-performance pseudocapacitors. *Angewandte Chemie International Edition*, 52(7), 1882-1889.
- [17]. Lyu, L., Chai, H., Seong, K. D., Lee, C., Kang, J., Zhang, W., & Piao, Y. (2018). Yeast-derived N-doped carbon microsphere/polyaniline composites as high performance pseudocapacitive electrodes. *Electrochimica Acta*, 291, 256-266.
- [18]. Okonkwo, P. C., Collins, E., & Okonkwo, E. (2017). Application of biopolymer composites in supercapacitor. In *Biopolymer composites in electronics* (pp. 487-503). Elsevier.
- [19]. Jeevanandam, J., Barhoum, A., Chan, Y. S., Dufresne, A., & Danquah, M. K. (2018). Review on nanoparticles and nanostructured materials: history, sources, toxicity and regulations. *Beilstein journal of nanotechnology*, 9(1), 1050-1074.
- [20]. Kumar, N., & Kumbhat, S. (2016). *Essentials in nanoscience and nanotechnology*. John Wiley & Sons.
- [21]. Gleiter, H. (2000). Nanostructured materials: basic concepts and microstructure. *Acta materialia*, 48(1), 1-29.
- [22]. Tiwari, J. N., Tiwari, R. N., & Kim, K. S. (2012). Zero-dimensional, one-dimensional, two-dimensional and three-dimensional nanostructured materials for advanced electrochemical energy devices. *Progress in Materials Science*, 57(4), 724-803.

- [23]. Pokropivny, V. V., & Skorokhod, V. V. (2007). Classification of nanostructures by dimensionality and concept of surface forms engineering in nanomaterial science. *Materials Science and Engineering: C*, 27(5-8), 990-993.
- [24]. Hochella, M. F., Spencer, M. G., & Jones, K. L. (2015). Nanotechnology: nature's gift or scientists' brainchild?. *Environmental Science: Nano*, 2(2), 114-119.
- [25]. Wagner, S., Gondikas, A., Neubauer, E., Hofmann, T., & von der Kammer, F. (2014). Spot the difference: engineered and natural nanoparticles in the environment—release, behavior, and fate. *Angewandte Chemie International Edition*, 53(46), 12398-12419.
- [26]. Izadi-Najafabadi, A., Yasuda, S., Kobashi, K., Yamada, T., Futaba, D. N., Hatori, H., ... & Hata, K. (2010). Extracting the full potential of single-walled carbon nanotubes as durable supercapacitor electrodes operable at 4 V with high power and energy density. *Advanced Materials*, 22(35), E235-E241.
- [27]. Zhang, L. L., & Zhao, X. S. (2009). Carbon-based materials as supercapacitor electrodes. *Chemical Society Reviews*, 38(9), 2520-2531.
- [28]. Shao, Y., El-Kady, M. F., Wang, L. J., Zhang, Q., Li, Y., Wang, H., ... & Kaner, R. B. (2015). Graphene-based materials for flexible supercapacitors. *Chemical Society Reviews*, 44(11), 3639-3665.
- [29]. Li, Q., Mahmood, N., Zhu, J., Hou, Y., & Sun, S. (2014). Graphene and its composites with nanoparticles for electrochemical energy applications. *Nano Today*, 9(5), 668-683.

- [30]. Tabrizi, A. G., Arsalani, N., Mohammadi, A., Ghadimi, L. S., & Ahadzadeh, I. (2018). High-performance asymmetric supercapacitor based on hierarchical nanocomposites of polyaniline nanoarrays on graphene oxide and its derived N-doped carbon nanoarrays grown on graphene sheets. *Journal of colloid and interface science*, *531*, 369-381.
- [31]. Meng, Q., Cai, K., Chen, Y., & Chen, L. (2017). Research progress on conducting polymer based supercapacitor electrode materials. *Nano Energy*, *36*, 268-285.
- [32]. Zheng, J., Zhang, R., Cheng, K., Xu, Z., Yu, P., Wang, X., & Niu, S. (2019). Research on the high-performance electrochemical energy storage of a NiO@ ZnO (NZO) hybrid based on growth time. *Crystals*, *9*(1), 47.
- [33]. Kim, B. K., Sy, S., Yu, A., & Zhang, J. (2015). Electrochemical supercapacitors for energy storage and conversion. *Handbook of clean energy systems*, 1-25.
- [34]. Holladay, J. D., Hu, J., King, D. L., & Wang, Y. (2009). An overview of hydrogen production technologies. *Catalysis today*, *139*(4), 244-260.
- [35]. Wang, S., Lu, A., & Zhong, C. J. (2021). Hydrogen production from water electrolysis: role of catalysts. *Nano Convergence*, *8*(1), 1-23.
- [36]. Scheepers, F., Stähler, M., Stähler, A., Rauls, E., Müller, M., Carmo, M., & Lehnert, W. (2020). Improving the efficiency of PEM electrolyzers through membrane-specific pressure optimization. *Energies*, *13*(3), 612.
- [37]. Dotan, H., Landman, A., Sheehan, S. W., Malviya, K. D., Shter, G. E., Grave, D. A., ... & Grader, G. S. (2019). Decoupled hydrogen and oxygen evolution by a two-step

electrochemical–chemical cycle for efficient overall water splitting. *Nature Energy*, 4(9), 786-795.

[38]. Symes, M. D., & Cronin, L. (2013). Decoupling hydrogen and oxygen evolution during electrolytic water splitting using an electron-coupled-proton buffer. *Nature chemistry*, 5(5), 403-409.

[39]. Hu, E., Feng, Y., Nai, J., Zhao, D., Hu, Y., & Lou, X. W. D. (2018). Construction of hierarchical Ni–Co–P hollow nanobricks with oriented nanosheets for efficient overall water splitting. *Energy & Environmental Science*, 11(4), 872-880.

[40]. Wang, W., Xu, M., Xu, X., Zhou, W., & Shao, Z. (2020). Perovskite oxide based electrodes for high-performance photoelectrochemical water splitting. *Angewandte Chemie International Edition*, 59(1), 136-152.

[41]. Tee, S. Y., Win, K. Y., Teo, W. S., Koh, L. D., Liu, S., Teng, C. P., & Han, M. Y. (2017). Recent progress in energy-driven water splitting. *Advanced science*, 4(5), 1600337.

[42]. Carrette, L., Friedrich, K. A., & Stimming, U. (2001). Fuel cells-fundamentals and applications. *Fuel cells*, 1.

[43]. Kanchev, H., Lu, D., Colas, F., Lazarov, V., & Francois, B. (2011). Energy management and operational planning of a microgrid with a PV-based active generator for smart grid applications. *IEEE transactions on industrial electronics*, 58(10), 4583-4592.

- [44]. Levard, C., Hotze, E. M., Lowry, G. V., & Brown Jr, G. E. (2012). Environmental transformations of silver nanoparticles: impact on stability and toxicity. *Environmental science & technology*, 46(13), 6900-6914.
- [45]. Xi, W., Phan, H. T., & Haes, A. J. (2018). How to accurately predict solution-phase gold nanostar stability. *Analytical and bioanalytical chemistry*, 410(24), 6113-6123.
- [46]. Shrestha, B. K., & Haes, A. J. (2015). Improving surface enhanced Raman signal reproducibility using gold-coated silver nanospheres encapsulated in silica membranes. *Journal of Optics*, 17(11), 114017.
- [47]. Szabo, P., & Zelko, R. (2015). Formulation and stability aspects of nanosized solid drug delivery systems. *Current pharmaceutical design*, 21(22), 3148-3157.
- [48]. Do, K. H., & Jang, S. P. (2010). Effect of nanofluids on the thermal performance of a flat micro heat pipe with a rectangular grooved wick. *International Journal of Heat and Mass Transfer*, 53(9-10), 2183-2192.
- [49]. Do, K. H., & Jang, S. P. (2010). Effect of nanofluids on the thermal performance of a flat micro heat pipe with a rectangular grooved wick. *International Journal of Heat and Mass Transfer*, 53(9-10), 2183-2192.
- [50]. Wagers, K., Chui, T., & Adem, S. (2014). Effect of pH on the stability of gold nanoparticles and their application for melamine detection in infant formula. *IOSR J. Appl. Chem*, 7, 15-20.

- [51]. Ma, R., Levard, C., Michel, F. M., Brown Jr, G. E., & Lowry, G. V. (2013). Sulfidation mechanism for zinc oxide nanoparticles and the effect of sulfidation on their solubility. *Environmental science & technology*, 47(6), 2527-2534.
- [52]. Ruíz-Baltazar, A., Esparza, R., Rosas, G., & Pérez, R. (2015). Effect of the surfactant on the growth and oxidation of iron nanoparticles. *Journal of nanomaterials*, 2015.
- [53]. Tahir, Muhammad & Pan, Lun & Idrees, Faryal & Zhang, Xiangwen & Wang, li & Zou, Ji-Jun & Wang, Zhong. (2017). Electrocatalytic Oxygen Evolution Reaction for Energy Conversion and Storage: A Comprehensive Review. *Nano Energy*. 37. 10.1016/j.nanoen.2017.05.022.
- [54]. Zou, X., & Zhang, Y. (2015). Noble metal-free hydrogen evolution catalysts for water splitting. *Chemical Society Reviews*, 44(15), 5148–5180. <https://doi.org/10.1039/c4cs00448e>